Agricultural Systems 233 (2026) 104635

Contents lists available at ScienceDirect

Agricultural Systems

journal homepage: www.elsevier.com/locate/agsy

Develop a modelling framework to identify and optimize the dominant factors that limit cropland productivity

Xiaoyang Han [a], Changqing Song [b,a], Leina Zhang [c], Peichao Gao [a], Sijing Ye [a,*], Yakov Kuzyakov [d,e]

[a] Faculty of Geographical Science, Beijing Normal University, Beijing 100875, China
[b] Faculty of Geogarphy, Yunnan Normal University, Yunnan 650500, China
[c] China land surveying and planning institute, Beijing 100035, China
[d] Department of Soil Science of Temperate Ecosystems, Department of Agricultural Soil Science, University of Goettingen, 37077 Göttingen, Germany
[e] Peoples Friendship University of Russia (RUDN University), 117198 Moscow, Russia

HIGHLIGHTS

- Mechanisms of the effects of farming conditions on cropland productivity were analyzed.
- Key limiting factors and their triggering conditions to cropland productivity were identified.
- Framework applicable to scenarios lacking high-precision crop yield were developed.
- Annual cropland productivity increased by 7% through adjusting soil texture and mean field size.

GRAPHICAL ABSTRACT

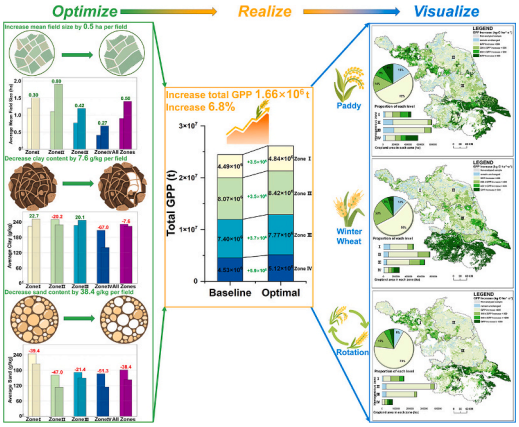

ARTICLE INFO

Keywords:
Land use
Soil quality
Cropland productive capacity
GPP
Land consolidation

ABSTRACT

Context: Analysing the influence mechanism of farming conditions (soil properties and agricultural infrastructure) on cropland productivity is a key prerequisite for increasing yields in low- to medium-quality land.
Objective: We proposed a modelling framework to identify key farming condition factors that limit cropland productivity and analyse the numerical ranges within which they exert a dominant influence. The responses of cropland productivity to changes in dominant farming conditions were simulated.
Methods: The framework consisted of processed long-term sequence earth observation data and random forest model. By filtering high-density cropland samples and increasing crop identification accuracy, gross primary production (GPP) was proven to be an appropriate indicator of cropland productivity in scenarios lacking high-precision crop yield data.

* Corresponding author at: Faculty of Geographical Science, Beijing Normal University, Beijing 100875, China.
E-mail address: yesj@bnu.edu.cn (S. Ye).

https://doi.org/10.1016/j.agsy.2026.104635
Received 30 September 2025; Received in revised form 23 November 2025; Accepted 7 January 2026
Available online 21 January 2026

Results and conclusions: Farming conditions explained >60% of the spatial differences in the rice GPP and > 65% of those in the wheat GPP. Soil texture and pH were key factors limiting rice and wheat GPP. A decrease in sand content and a corresponding increase in clay content increased rice GPP. Soil nitrogen supply rapidly decreased when clay content approached 20%, decreasing rice GPP. Climate conditions influenced the preference of wheat for soil water retention and drainage-permeability, resulting in an increase wheat GPP in northern and decrease in southern regions with raising clay content. The annual total GPP of rice and wheat increased by up to 6.8% through adjusting clay and sand contents and increasing mean field size. In the northwestern and southeastern regions, small adjustments (−5% … +5%) to clay and sand contents led to annual GPP increases of >600 kg·C·ha^{-1} for rice and > 800 kg·C·ha^{-1} for paddy-wheat rotations.
Significance: The framework can provide support to optimize farming conditions in low- to medium-yield cropland renovation projects.

1. Introduction

Croplands constitute the material foundation for human survival and development, providing multiple ecosystem functions, such as food, fodder and material production; climate regulation; biodiversity conservation; water purification; and cultural heritage (Foley et al., 2011; Viana et al., 2022; Du et al., 2024). The ability of croplands to supply food, feed, fibre, and other agricultural products (i.e., productive functions) is central (Ye et al., 2023). In localized farming scenarios characterized by specific climatic conditions and crop types, the cropland productive function (productivity) is mainly constrained by land surface farming conditions (including topographic position, soil properties, and farmland infrastructure) (Ye et al., 2019). Increasing the productivity of low- and medium-yield cropland through land consolidation and soil improvement projects has crucial implications for food security, ecological stability and climate change (Ren et al., 2022; Ye et al., 2020, 2022a, 2022b; Liu et al., 2023). A key prerequisite for the rational implementation of these projects is a comprehensive understanding of the influence of farming conditions on cropland productivity.

The lack of long-term and local data makes it difficult to study the influences of farming conditions on cropland productivity at the regional scale and over long periods (Ye et al., 2022a). Methods for depicting cropland productivity mainly include field sampling and model-based approaches. Field sampling methods have the advantages of being straightforward and highly accurate, and these methods provide essential site-specific data for model-based estimations of cropland productivity. Due to high economic and labour costs, the application of field sampling methods has been restricted (Fang et al., 2008; Ye et al., 2014).

Model-based approaches primarily include spectral regression models, crop mechanistic models, and assimilation models. Spectral regression models estimate cropland productivity by establishing regression relationships between vegetation indices and measured crop yields (Yang and Everitt, 2012; Deines et al., 2021). For example, Bolton and Friedl (2013) noted that the enhanced vegetation index measured at specific crop growth dates (e.g., 65–75 days after green up for maize) was closely linearly correlated with crop yield ($R^2 \geq 0.67$) (Bolton and Friedl, 2013). The regression between spectral features and crop yields depend on both crop and environmental factors, including crop variety and climate and soil properties. This specificity poses challenges for the widespread application of spectral regression models, as high-quality crop yield data are needed across multiple homogeneous environmental zones.

For crop mechanistic models (e.g., APSIM), a set of differential equations is constructed to simulate the accumulation and allocation of crop dry matter under specific environmental conditions (Hu et al., 2024). Compared with spectral regression models, crop mechanistic models require few point-specific crop yield data but demand more detailed environmental parameters. Cases in which crop mechanistic models are applied over a large scale to simulate grid-based approximations of actual crop yields, as executed by Xiao et al. (2024), are rare. In most studies, crop potential yield, which is simulated by several assumed environmental parameters (e.g., adequate water or nitrogen supply), is used to indicate cropland productivity (Ye et al., 2022a; Xiao et al., 2024). Crop yields (or biomass) estimated solely by crop mechanistic models, however, are unsuitable dependent variables for analysing how farming conditions influence cropland productivity. Because the effects of farming conditions on crop yield are prespecified in the model equations.

Assimilation models provide a way to blend the monitoring of crop spectral information with the predictive and explanatory strengths of crop mechanistic models (Huang et al., 2015, 2019, 2023). As a typical assimilation model, the MODIS gross primary productivity (GPP) model (i.e., MODIS-PSN) is widely used to represent long-term cropland productivity, offering high temporal resolution, wide coverage, and high availability, especially in the absence of high-quality crop yield data (Running et al., 2004). For example, Khan et al. (2024) used MODIS GPP time series data from the U.S. Midwest corn belt as input, achieving high accuracy in county-level simulations for corn ($R^2 = 0.86$) and soybeans ($R^2 = 0.75$).

Soil quality studies accumulated extensive knowledge and cases to the effects of farming conditions on cropland productivity. Due to the complexity and spatial heterogeneity of the driving mechanisms of soil functions, single indicators are insufficient to reflect changes in soil functions (Liu et al., 2006). Larson and Pierce (1991) introduced the concept of a minimum dataset (MDS), which aims to reflect soil functions by using the most critical physical, chemical, and biological indicators (Paustian et al., 1997; Halvorson et al., 2002; Lal, 2018). The soil quality index area approach was developed to combine chemical, biological and physical soil properties as areas on a radar diagram to assess soil degradation and recovery (Guillaume et al., 2016; Kuzyakov et al., 2020; Gao et al., 2023).

Weighted averaging methods are typically applied to calculate the comprehensive soil quality index (SQI) (Doran and Parkin, 1994; Rinot et al., 2019). Methods for determining indicator weights can be categorized into three types: expert prior knowledge-based methods (e.g., the Delphi method, analytic hierarchy process) (Ye et al., 2014, 2019); methods based on indicator feature analysis (e.g., the entropy weight method, frequency (FR) method, principal component analysis) (Zhou et al., 2016; Ren et al., 2023); and causal inference- or regression-based methods (e.g., geographic detectors, structural equation models, random forest models) (Wang and Zhang, 2013; Wang, 2017; Du et al., 2024). The process of determining the weights of soil quality indicators can reveal the dominant factors affecting soil functions. For example, Obade and Lal (2016) collected 204 soil samples from five private farms in Ohio and used reduced regression, principal component regression, and partial least squares regression to analyse the interactions among 10 soil physicochemical indicators. The results revealed that soil organic carbon, bulk density, C:N ratio, and electrical conductivity were the most influential variables affecting soil productivity (Obade and Lal, 2016). Swanepoel et al. (2014) used principal component analysis to extract key indicators affecting soil quality, including available phosphorus, gravel content, water-holding capacity, exchangeable acidity, and organic matter, in 142 kikuyu and ryegrass pasture systems in South

Africa.

Studies on the weights of soil quality indicators, however, still face limitations in characterizing their influence mechanisms on cropland productivity. Expert knowledge-based methods can capture the generally dominant soil quality factors that influence cropland productivity but struggle to identify the limiting factors and their thresholds in localized areas (Ye et al., 2019; Wan et al., 2021). Methods based on indicator feature analysis estimate the weights of soil quality indicators based on the magnitude and direction of their changes (Ren et al., 2023). These methods are subject to high uncertainty since changes in soil indicators do not necessarily drive differences in cropland productivity. Although some causal inference or regression methods (e.g., structural equation models and geographic detectors) offer explanations for diagnosing the dominant factors affecting cropland productivity, they are still limited because of a lack of appropriate dependent variable data (Duflot et al., 2022; Gong et al., 2022). For example, in multiple regression model-based studies, the soil quality index has been used as the dependent variable to represent cropland productivity (Paul et al., 2020; Fathizad et al., 2020; Liu et al., 2020b). When this scheme is applied to analyse the mechanisms of soil quality effects on cropland productivity, the preassigned weights used to calculate the SQI inevitably interfere with the research outcomes.

The aim of this study was to develop a modelling framework to identify key farming condition factors that limit cropland productivity and analyse the numerical ranges within which they exert a dominant influence in scenarios lacking high-precision crop yield data. A scheme combining GPP data with random forest has been proposed. By dividing the climate homogeneous zones and extracting the high density — same crop type grids, the disturbances to the model's accuracy, which caused by the differences in climate condition and crop types as well as the mixed land use types, have been reduced. A typical grain-producing province in the plain area of China (i.e., Jiangsu Province) was selected as the study area to mitigate the influence of spatial differences in cropland use practices (e.g., chemical input intensity and agricultural mechanization). The annual cumulative GPP corresponding to the crop growth periods of rice and wheat were extracted at the 1 km grid level to serve as an indicator of cropland productivity from 2001 to 2020. The influences of changes in farming conditions on cropland productivity in paddy and wheat fields were analyzed by using random forest. The responses of cropland productivity per unit area to changes in dominant farming conditions were subsequently simulated. The discussion section presents an analysis of the uncertainties of the proposed framework and further explains how farming conditions affect cropland productivity. The framework can provide technical support to optimize farming conditions in low- to medium-yield cropland renovation projects and future national arable land quality assessment projects in China.

2. Data and methodology

2.1. Study area

Jiangsu Province is a major grain-producing province in China and is located in the lower reaches of the Yangtze and Huai Rivers (116°18′–121°57′E, 30°45′–35°20′N) (Fig. 1). Plains cover nearly 87% of the total Jiangsu Province. Most parts of Jiangsu Province have elevations less than 50 m, providing extensive arable land for agricultural production.

Climatically, Jiangsu Province lies within the East Asian monsoon region and is situated in the transitional zone between warm temperate and subtropical monsoon climates, with average annual temperatures ranging from 13.6 to 16.1 °C and annual precipitation between 700 and 1250 mm (Jiangsu Provincial Bureau of Statistics, 2023). The southern part of Jiangsu Province receives abundant rainfall, whereas the northern part is relatively dry. The abundant light and heat conditions, sufficient depth of the arable horizon, and well-structured soils support intensive cropland use in the study area. In terms of land use, Jiangsu Province has 4.1 million hectares of cropland, accounting for approximately 3.2% of China's total cropland area, and has a highly contiguous distribution (Office of the Third National Land Survey Leading Group of the State Council, Ministry of Natural Resources, National Bureau of Statistics, 2021). Paddy and wheat (including paddy-wheat rotation) is the predominant cropping pattern in Jiangsu Province. According to the 2024 China Statistical Yearbook and Jiangsu Statistical Yearbook, the annual sowing areas of paddy and wheat in Jiangsu Province reached 22,210 km^2 and 23,895 km^2, covering 84.5% of the total sown area of cereal, tuber and legume crops, with average yields of 5750 $kg{\cdot}ha^{-1}$ and 9020 $kg{\cdot}ha^{-1}$. Notably, the high level of mechanization and well-developed cropland infrastructure throughout Jiangsu Province has resulted in generally high land use intensity with low spatial heterogeneity (Ye et al., 2020). Take Jiangsu Province as the study area helps mitigate the influence of spatial differences in cropland use practices (e.g., chemical input intensity and agricultural mechanization).

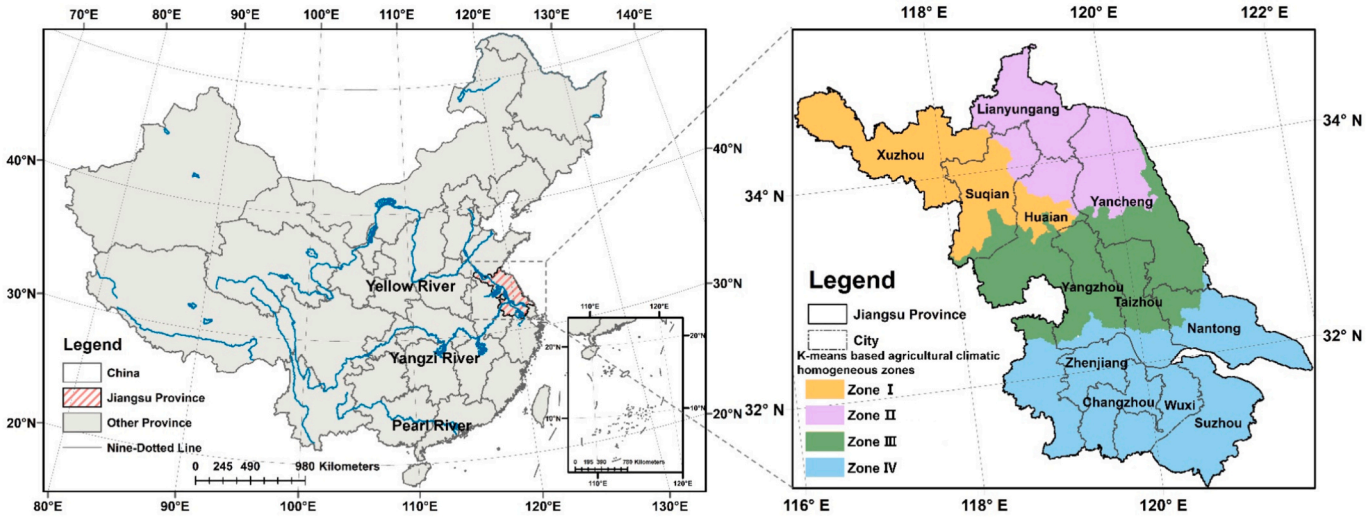

Fig. 1. Geographical location and agricultural climatic zones of the study area. The K-means method was used to divide the study area into four agricultural climatic zones: warm temperate continental monsoon zone (zone I), warm temperate oceanic monsoon zone (zone II); north subtropical monsoon zone (zone III), and central subtropical monsoon zone (zone IV).

2.2. Data processing

This study involves four main types of datasets. The first type comprises 1 km resolution monthly data of maximum temperature, minimum temperature, mean temperature, and total precipitation for the period 1991–2020. These meteorological data were sourced from a 1 km monthly temperature and precipitation dataset for China (1901–2023) (Peng et al., 2019). For each month, the multiyear average of the monthly average temperature, monthly maximum temperature, monthly minimum temperature and monthly total precipitation were calculated and fed into the K-means method to divide the study area into four agricultural climatic homogenous zones (*see detailed information on K-means-based agricultural climatic homogenous zones in Appendix A.1*). Subsequent analyses of the influence of farming conditions on cropland productivity were performed separately within each agricultural climatic homogeneous zone to mitigate the effects of climatic variability on crop GPP.

The second type of dataset characterizes cropland productivity. The annual 500 m MODIS 8-day GPP product (MOD17A2H raster dataset) from 2001 to 2020 was used as the data source (Running et al., 2004). For each year, in 1 km resolution grids, where paddy or wheat was predominantly grown, the cumulative GPP during the paddy growth period (Days 161 to 321 of the current year) and the wheat growth period (from Day 321 of the previous year to Day 137 of the current year) was upscaled to 1 km resolution and used as an indicator of cropland productivity. Three-standard deviation-based GPP outlier detection was applied to mitigate the impact of extreme weather events on crop GPP.

The third type of dataset was used to identify 1 km resolution grids with high-density paddy or wheat cultivation. This includes the GlobeLand30 raster datasets for 2000, 2010, and 2020 (Chen et al., 2014, 2015) and a dataset of the planting areas of three staple crops in China during 2009–2015 (Mei et al., 2023). To mitigate the interference of other land-use types mixed within the 1 km resolution grids on crop GPP, 1 km grid-based cropland densities (i.e., the ratio of cropland area to grid area) in 2000, 2010 and 2020 were calculated from the GlobeLand30 dataset. Grids with cropland densities above 95% in 2000, 2010, and 2020 were extracted as the base sample set, which mitigated the interference of newly added cropland with relatively poor cultivation infrastructure conditions on crop GPP. The 2009–2015 annual crop type raster dataset (Mei et al., 2023) was overlaid to extract grids cultivated with wheat and paddy from the base sample set, outputting initial annual sample sets for these crops. The dynamic time warping (DTW) method was used to refine these sample sets to reduce uncertainties arising from crop type identification errors (*see detailed information on DTW-based sample set cleaning in Appendix A.2*).

The fourth type of dataset comprises indicator data on farming conditions that affect cropland productivity, including soil property indicators and utilization condition indicators. Soil property indicators are sourced from the high-resolution national soil information grid dataset for China (2010–2018) (Liu et al., 2020a, 2022) (Table 1). The utilization condition indicators consist of measures of cropland fragmentation (e.g., mean field size, area-weighted mean shape index) and cropland infrastructure conditions (e.g., irrigation guarantee level, drainage conditions). Data related to the utilization condition indicators were derived from the Ministry of Natural Resources' pilot survey on arable land quality and productive capacity (Ye et al., 2019, 2024b; Zhang et al., 2024). Collinearity diagnostics indicated that, after removing the silt content, the variance inflation factors for the remaining indicators were all less than 10. Detailed data source information is presented in Table 1. The research process is illustrated in Fig. 2.

2.3. Simulating the response of GPP to changes in soil texture and mean field size

In each agricultural climatic homogeneous zone, a random forest model was trained using the 2020 GPP of the paddy field and wheat field grids as the dependent variable. The GPP for paddy and wheat fields within their cultivation grids was simulated as the baseline scenario

Table 1
Detailed dataset information.

Categories	Indicators	Explanations	Data Source	Spatial resolution	Year
Climate Data	PR	Monthly precipitation (mm)	1 km monthly temperature and precipitation dataset for China from 1901 to 2023 (Peng et al., 2019)	1 km	1991–2020
	MAT	Monthly maximum temperature (°C)			
	MET	Mean monthly temperature (°C)			
	MIT	Monthly minimum temperature (°C)			
Cropland Productive Function Dataset	GPP	Gross Primary Productivity ($kg{\cdot}C{\cdot}ha^{-1}$)	MODIS 8 day-GPP MOD17A2H raster dataset (Running et al., 2004)	500 m	2001–2020
Land Use Type and Crop Type Raster Dataset	Cropland Density	Percentage of cropland area relative to the total area within a 1 km grid cell (%)	GlobeLand30 raster dataset (Chen et al., 2014, 2015)	1 km	2000, 2010, 2020
	–	Paddy type raster dataset	A dataset of the planting areas of three staple crops in China (Mei et al., 2023)	1 km	2009–2015
	–	Winter wheat type raster dataset			
Soil Properties	BD	Soil bulk density ($g{\cdot}cm^{-3}$)	Basic soil property dataset of high-resolution China Soil Information Grids (2010–2018) (Liu et al., 2020a, 2020b, 2022, weighted average value over the 0–30 cm depth	1 km	2010–2018
	ST	Soil thickness (mm)			
	GC	Gravel content (%)			
	CLY	Clay content (%)			
	SND	Sand content (%)			
	pH	Soil pH			
	SOC	Soil organic carbon content ($g{\cdot}kg^{-1}$)			
	CEC	Cation exchange capacity ($cmol{\cdot}kg^{-1}$)			
	TK	Total potassium ($g{\cdot}kg^{-1}$)			
	TN	Total nitrogen ($g{\cdot}kg^{-1}$)			
	TP	Total phosphorus ($g{\cdot}kg^{-1}$)			
Cropland Fragmentation Degree	MFS	Mean field size (ha)	China's Second National Land Use Survey (Ye et al., 2024a, 2024b; Zhang et al., 2024)	1 km	2010
	AWMSI	Area-weighted mean shape index			
Cropland Infrastructure Conditions	DFN	Forest Network Condition	Pilot Survey Project of Cropland Land Quality and Productivity of the Ministry of Natural Resources (Ye et al., 2019)	1 km	2018
	AML	Agricultural Mechanization Level			
	DC	Drainage Condition			

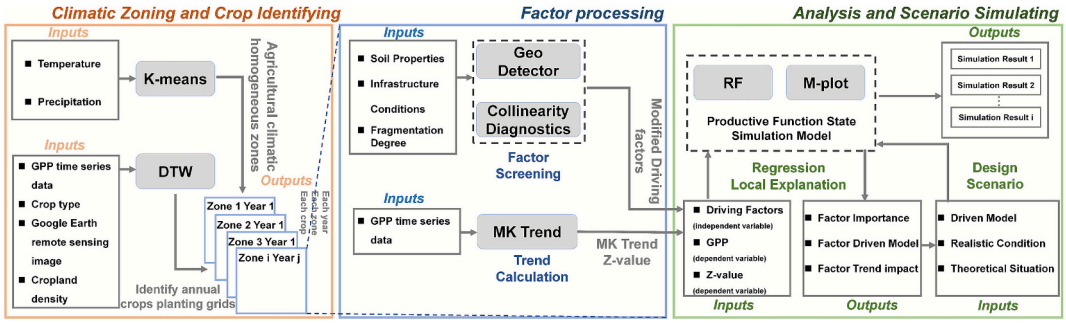

Fig. 2. Flowchart of the research processes. The agricultural climatic homogeneous zoning stage involves: using the K-means method to divide the study area into 4 zones with similar temperature and precipitation characteristics (see Fig. 1); using dynamic time warping (DTW) to verify the annual crop planting grids. Factor processing stage focused on factors selection through collinearity diagnostics and geographic detectors and employed the Mann–Kendall (MK) trend test to analyse the 20-year interannual variation in gross primary productivity (GPP). In the identification and simulation modelling stage, a random forest model and marginal plots were used to analyse the importance of factors and their influences on cropland productivity. The random forest model was subsequently used to simulate crop land productivity under various scenarios of soil texture and mean field size adjustments.

(*Fig. S.11*). Then, for each grid, other farming condition factors were held constant, and the maximum GPP under combined scenarios of varying clay content, sand content and increased mean field size was simulated as the optimal scenario. For a given grid i, the clay content C_i was varied from [0.5*C_i, 1.5*C_i] in 4%*C_i increments; the sand content S_i was varied from [0.5*S_i, 1.5*S_i] in 4%*S_i increments; and the mean field size M_i (unit: ha) was varied from [M_i, $M_i + 3$] in 0.12 ha per field increments. The 4% step was chosen to create 25 evenly spaced variants within each variable's feasible range, ensuring a balance between computational efficiency and sensitivity resolution. During each adjustment, the total proportion of sand, silt, and clay was constrained to 100%, with the silt fraction computed as 100% − (clay + sand). The optimization was conducted synchronously, with clay content, sand content, and mean field size jointly varied within their respective ranges for each grid to determine the combination yielding the maximum simulated GPP. Based on actual 2020 cropping patterns, 30 m resolution grids were classified into paddy-only, wheat-only, and paddy-wheat rotations by overlaying the 30 m wheat dataset (Dong et al., 2020) and the 10 m paddy field dataset (Pan et al., 2021). Sown areas were then aggregated into 1 km grids. For the paddy-wheat rotation type, the GPP was defined as the sum of the GPP of the paddy and wheat fields. According to statistics from the wheat (Dong et al., 2020) and paddy field (Pan et al., 2021) datasets, the sown areas in Jiangsu were 25,620 km^2 for paddy fields and 21,470 km^2 for wheat in 2020, deviating by 16.3% and 8.2%, respectively, from the Jiangsu Statistical Yearbook. The areas of paddy-only (17,070 km^2), wheat-only (12,920 km^2), and paddy-wheat rotation (8550 km^2) cropland accounted for 41.6%, 31.5%, and 20.8% of the total cropland area in the study region.

2.4. Geodetector method

Geodetector is a statistical method based on the theory of spatial stratification and is designed to detect heterogeneity in stratified sample spaces and reveal the underlying driving forces (Wang et al., 2010; Wang and Hu, 2012; Wang et al., 2016). This method is commonly used to attribute the driving effects of independent variables to the spatial distributions of dependent variables (Wang et al., 2024; Zhou et al., 2020). In the Geodetector method, the q value is used to measure the explanatory power of an independent variable on the dependent variable (Eq. (1)). In the formula, l represents the number of strata, N_h represents the sample size in stratum h, and σ_h^2 represents the variance within stratum h. The q value ranges from 0 to 1. A larger q indicates stronger explanatory power of the independent variable on the dependent variable.

The agricultural intensification level of cropland is generally high in Jiangsu Province, with low spatial heterogeneity under cropland infrastructure conditions. The geodetector method was used to examine the driving effect of cropland infrastructure indicators on cropland productivity. The q values for the cropland infrastructure indicators in the four climatic homogeneous zones were extremely low ($q < 0.05$) and nonsignificant ($p > 0.05$) (Table 3). This suggests that the influence of infrastructure conditions on cropland productivity is weak. Consequently, cropland infrastructure indicators were excluded from the subsequent analysis.

$$q = 1 - \frac{\sum_{h=1}^{l} N_h \sigma_h^2}{N\sigma^2} \cdots \quad (1)$$

2.5. Mann–Kendall trend test

The Mann–Kendall test was used to analyse the trend of cropland productivity changes in each grid of paddy fields or wheat fields from 2001 to 2020. The Mann–Kendall test is a nonparametric method for analysing trends in time series data (Mann, 1945). This method does not require the sample data to follow a normal distribution and is robust against outliers. According to the formulas of the Mann–Kendall test (Eq. (2), Eq. (3)), $sgn(X_i - X_j)$ denotes the sign function. X_i and X_j represent the current and preceding values in the time series. The standardized test statistic (Z-value) is used to assess the trend and its significance in the time series (Eq. (4)). A Z-value >0 indicates an upwards trend, whereas a Z-value<0 indicates a downwards trend. The absolute Z-values of 1.645, 1.96, and 2.576 correspond to significance levels of 90%, 95%, and 99%.

$$S = \sum_{i=2}^{n} \sum_{j=1}^{i-1} sgn(X_i - X_j) \cdots \quad (2)$$

$$Var(S) = \frac{n(n-1)(2n+5)}{18} \cdots \quad (3)$$

$$\text{Z} - \text{value} = \begin{cases} \dfrac{S-1}{\sqrt{Var(S)}} & S > 0 \\ 0 & S = 0 \\ \dfrac{S+1}{\sqrt{Var(S)}} & S < 0 \end{cases} \cdots \quad (4)$$

3. Results

3.1. Spatiotemporal specifics of cropland productivity

Cropland productivity, which is indicated by the average GPP (Fig. 3 a–b), follows an approximately normal distribution. It has a spatial

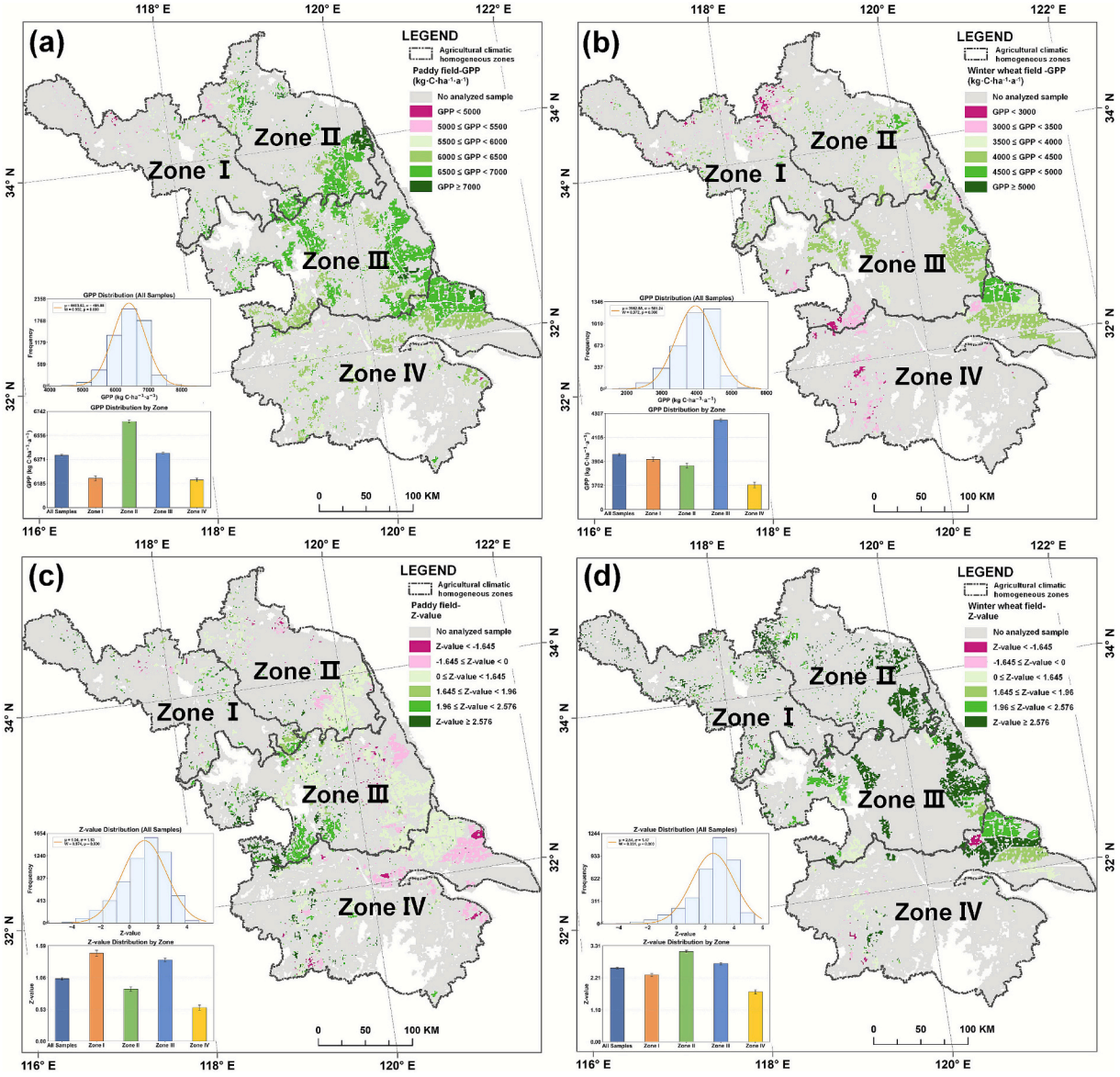

Fig. 3. Spatial patterns and temporal trends of cropland productivity. Only grids with cropland density above 95% are displayed. The sample count was 6395 for paddy fields and 3859 for wheat fields. (a) Average GPP of paddy fields at 1 km resolution during 2001–2020; (b) average GPP of wheat fields at 1 km resolution during 2001–2020; (c) Mann–Kendall Z-value of paddy fields at 1 km resolution during 2001–2020; (d) Mann–Kendall Z-value of winter wheat fields at 1 km resolution during 2001–2020. A Z-value > 1.645 indicates an upward trend ($p < 0.1$); a Z-value < −1.645 indicates a downward trend (p < 0.1). An increase in |Z − value| indicates a strengthening of the trend.

pattern of "high in the northeast–low in the southwest". Paddy fields with a mean GPP above 6500 kg·C·ha^{-1}·a^{-1} are located mainly in southeastern zone II and eastern zone III. Wheat fields with a mean GPP above 4000 kg·C·ha^{-1}·a^{-1} are concentrated along the eastern coast of zones III and IV. The northwestern region of zone II and the northwestern region of zone IV have the lowest average GPP for wheat fields.

The trend of cropland productivity follows a skewed normal distribution (Fig. 3 c–d). Driven by improved cultivars and advances in agricultural science and technology, both paddy fields and wheat fields experience clear increasing trends (for rice, the average Z value is 1.04; for wheat, the average Z value is 2.54). Some grids, however, have experienced declines in cropland productivity, especially in paddy fields. Paddy field productivity mainly increases in the west and decreases in the east. Zones I and the western part of zone III have strong upwards trends with high *Z*-values. The trend of the paddy field GPP in the eastern part of Jiangsu Province is non-significant (|Z-value| < 1.645). Most wheat fields show increases (|Z-value| > 1.645) in cropland productivity, particularly in the eastern regions of zones II and III. For paddy–wheat rotation grids, a decline in cropland productivity for one crop is not evidence of a decline for the other crop. In eastern Jiangsu Province, many grids with decreases (Z-value < −1.0) in paddy field GPP simultaneously show increases (Z-value >1.645) in wheat field GPP.

3.2. *Farming conditions affect the spatial differences in cropland productivity*

Farming conditions explain an average of 60.5% of the spatial differences in paddy field productivity and 65.6% of wheat field productivity (*see Interannual variation of Random Forest model based R^2 in the test sets in Fig. S.3*).

Soil texture (indicated by clay and sand contents) and pH are the most influential factors on paddy field productivity (Fig. 4a) (*see annual influence intensity in Fig. S.4*). Slightly acidic soils favor rice growth.

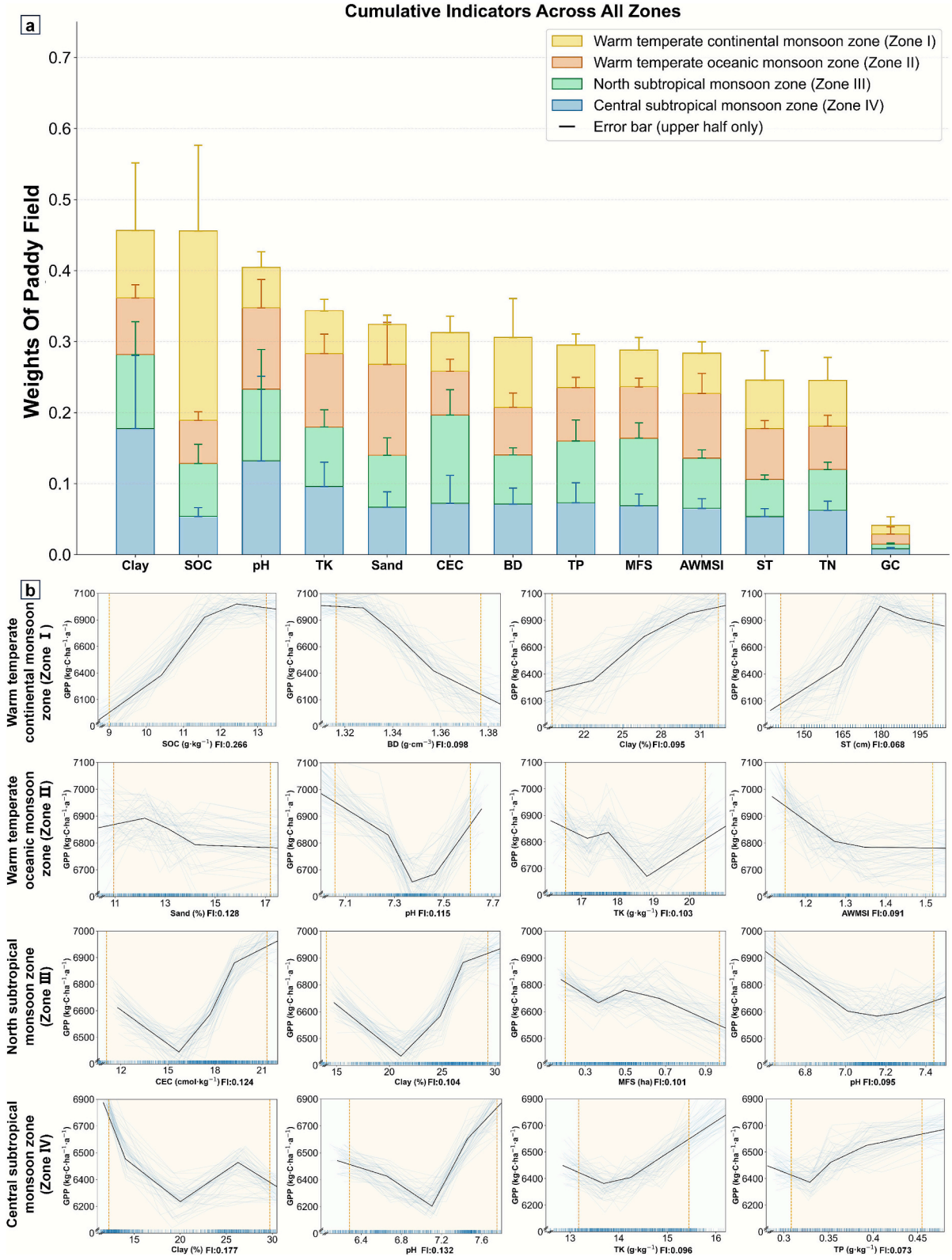

Fig. 4. Farming condition factors' importance and driving patterns on paddy field productivity. In Fig. 4(a), factors are sorted from left to right in descending order according to their cumulative influence intensity in all agricultural climatic homogeneous zones. Fig. 4(b) displays the response of paddy field GPP to changes in the four farming condition factors with the highest importance for each climatic homogeneous zone. FI is an abbreviation of "factor importance". To mitigate the interference of extreme values on the fitted M-plots, the influence ranges of each factor between the 10% and 90% quantiles are highlighted with a light orange background. The full names of each farming condition factor are as follows: BD (soil bulk density, g·cm^{-3}), GC (gravel content, %), AWMSI (area-weighted mean shape index), MFS (mean field size, ha), pH (soil pH), TN (total nitrogen, g·kg^{-1}), TK (total potassium, g·kg^{-1}), TP (total phosphorus, g·kg^{-1}), SOC (soil organic carbon content, g·kg^{-1}), ST (soil thickness, mm), CEC (cation exchange capacity, cmol·kg^{-1}), Sand (sand content, %), and Clay (clay content, %). *The annual influence intensity is shown in Fig. S.4. The response of paddy field productivity to changes in all farming condition factors is shown in Fig. S.6.*

Paddy field GPP declines as pH increases in all zones (Fig. 4b) (*see response of paddy field productivity to changes of each farming condition factor in Fig. S.6*). The decrease in paddy field GPP with increasing pH is most sensitive in zones III and IV (occurring in the pH range of 6.5–7.0). In the paddy fields with slightly alkaline soil in zones II, III and IV, an increase in pH corresponds to an increase in GPP. This pattern reflects the shift to alkali-tolerant, high-yield hybrid rice varieties in areas unsuitable for conventional varieties due to high pH.

The contents of sand, silt, and clay jointly influence the paddy field GPP. In most zones, increased sand content drives a decrease in GPP. In zone III, however, the increase in sand content coincides with an increase in clay content, which drives the increase in GPP in the paddy field (*Fig. S.7*). In grids with clay contents above 20%, an increase in the clay content contributes to an increase in rice GPP. Within the range of 10% to 20%, however, increased clay content sharply reduces the soil nitrogen supply capacity and consequently leads to a decrease in GPP (Zhang, 1988).

Total potassium has a higher influence in zones II and IV. Below 16 $g{\cdot}kg^{-1}$, increase in total potassium content contributes to GPP raise. When the total potassium content exceeds 16 $g{\cdot}kg^{-1}$, its increase drives down paddy field GPP. In the case of <0.5 $g{\cdot}kg^{-1}$, an increase in the soil total phosphorus content raise paddy field GPP, especially in zone IV. In zones I and II, phosphorus content above 0.51 $g{\cdot}kg^{-1}$ and 0.55 $g{\cdot}kg^{-1}$ result in decreases in GPP.

For paddy fields with a mean field size exceeding 0.5 ha, under the premise of maintaining current smallholder farming practices, further increases in the mean field size correspond to unchanged or even reduced GPP. Gravel content has a negligible influence across all climatic homogeneous zones.

Similar to paddy fields, soil texture and pH are the primary factors affecting wheat field productivity (Fig. 5a) (*see annual influence intensity in Fig. S.5*). An increase in pH leads to an increase in wheat GPP across all climatic homogeneous zones (Fig. 5b) (*see the response of wheat field productivity to changes in each farming condition factor in Fig. S.6*). For paddy–wheat rotation fields, the influence of pH on cropland productivity has a trade-off relationship.

In terms of soil texture, once the sand content exceeds 15%, an increase in the sand content leads to a decrease in the wheat field GPP. The wheat field GPP decreases as clay content increases in southern Jiangsu Province (i.e., zones III and IV), but it increases as clay increases in northern Jiangsu Province (i.e., zones I and II). Clay has the strongest influence on the wheat field GPP in zone IV, with an influence intensity of 0.31, which is 3 to 5.1 times of that in other zones. Wheat fields tolerate more total phosphorus than paddy fields do, but their tolerances to excess total potassium are similar. Excessive increases in total phosphorus ($>$ 0.6 $g{\cdot}kg^{-1}$) or total potassium ($>$ 16 $g{\cdot}kg^{-1}$) both lead to decreases in wheat field GPP. In the range of less than 1 ha per field, an increase in the mean field size corresponds to an increase in the wheat field GPP.

3.3. Farming conditions affect temporal changes in cropland productivity

Temporal changes in cropland productivity are driven primarily by external factors such as climate change, cultivar improvements, and advances in cultivation techniques. Farming conditions influence the response of cropland productivity to these external factors, thereby affecting the trends in cropland productivity.

The cross-validation results indicate that farming conditions explain 43–61% of the trend in paddy field productivity. Soil texture, pH, cropland fragmentation, cation exchange capacity, and soil organic C content are the primary factors (*see detailed farming condition factors' intensity in Fig. S.8*). In zone I, excessive sand content is the main constraint on the increase in GPP in paddy fields. An increase in the sand content within the 20–30% range decreases the *Z*-value (Fig. 6a) (*see Fig. S.10 for response curves of all factors*). A decrease in the area-weighted average shape index and an increase in the cation exchange capacity correspond to an inse in the Z-value. In zone II, cropland fragmentation is the primary factor influencing paddy field GPP trends. An increased area-weighted mean shape index greatly reduces the Z-value. Only in the low value range of the mean field size ($<$ 0.5 ha), its increase corresponds to an increase in the Z-value. The Z-value decreases as excessive increase in total potassium ($>$ 19 $g{\cdot}kg^{-1}$). In zone III, the soil pH and clay content are the main factors influencing the Z-value. Both decreased pH and increased clay content drive greater Z-values. An increase in the clay content within the 20–30% range corresponds to an increase in the Z-value. In the pH range of 6–7, increasing the pH results in a decrease in the Z-value.

The cross-validation results indicate that farming conditions explain 45–63% of the trend in wheat field productivity. In Zone I, the mean field size, pH, total potassium, and total phosphorus have important influences on the wheat field GPP trends (*see detailed intensity in Fig. S.9*). Within the range of $<$0.86 ha per field, an increase in the mean field size increases the Z-value (Fig. 6b). In fields with total potassium contents less than 16 $g{\cdot}kg^{-1}$, an increase in total potassium leads to an increase in the Z-value. In zone II, excessive total potassium is the main factor limiting the Z-value. An increase in total potassium above 16 $g{\cdot}kg^{-1}$ leads to a decrease in the Z-value. An increase in total phosphorus above 0.6 $g{\cdot}kg^{-1}$ leads to a decrease in the Z-value. In zone III, the Z-value increases with increases in total potassium, total phosphorus, and pH. In zone IV, the soil texture is the primary factor influencing the Z-value, and increases in both clay content and sand content decrease the Z-value.

3.4. Simulation of cropland productivity

The total annual GPP of paddy fields and wheat fields in Jiangsu Province can be raised from 2.45E+07 t to 2.61E+07 t through increasing mean field size and adjusting soil clay and sand contents (Fig. 7). This represents a net increase of 6.8% (or 1.66E+06 t). The increases in GPP in zones I–IV are 3.5E+05 t (7.8%), 3.5E+05 t (4.3%), 3.7E+05 t (5.0%), and 5.9E+05 t (13.1%). To achieve this target, the average mean field size in zone I–IV need be increased by 0.2 ha, 0.80 ha, 0.42 ha, and 0.27 ha per field. The clay content need be adjusted by $+23$ $g{\cdot}kg^{-1}$, -20 $g{\cdot}kg^{-1}$, $+20$ $g{\cdot}kg^{-1}$, and -67 $g{\cdot}kg^{-1}$. The average sand content need be adjusted by -39 $g{\cdot}kg^{-1}$, -47 $g{\cdot}kg^{-1}$, -21 $g{\cdot}kg^{-1}$, and -51 $g{\cdot}kg^{-1}$.

Compared with wheat fields, paddy fields have higher increase over wide areas (Fig. 8 a/d). 18% of paddy-only grids have annual GPP growth exceeding 600 $kg{\cdot}C{\cdot}ha^{-1}{\cdot}a^{-1}$. The paddy and paddy–wheat rotation grids with the highest increases are located mainly in zone I and the eastern region of zone IV. Wheat fields with high GPP optimization efficiency (exceeding 400 $kg{\cdot}C{\cdot}ha^{-1}{\cdot}a^{-1}$), accounting for 11% of the total sown area, are distributed mainly in zone IV.

In most grids, measures to optimize the soil sand and clay contents for paddy field GPP also result in synergistic gains in wheat field GPP (Fig. 8 b/e/h, *Fig. S.11*). In the eastern region of zone III, however, increasing the clay content to raise paddy field GPP limits the GPP gains in wheat and paddy-wheat rotation fields. In the southwestern region of zone I, the optimization directions of the clay content according to the GPP in paddy fields and wheat fields are the opposite.

The paddy field and paddy-wheat rotation field in zone I and the eastern region of zone IV have high optimization efficiencies (Fig. 8, *Fig. S.11*). In these areas, small adjustments to the soil sand and clay contents (-50 $g{\cdot}kg^{-1}$ to $+50$ $g{\cdot}kg^{-1}$) combined with increases in the mean field size generally yield GPP gains of more than 600 $kg{\cdot}C{\cdot}ha^{-1}{\cdot}a^{-1}$ in paddy fields and more than 800 $kg{\cdot}C{\cdot}ha^{-1}{\cdot}a^{-1}$ gains in paddy–wheat rotation fields. The eastern region of Zone IV has the greatest increase in GPP in paddy fields, which occurs after a substantial increase ($>$ 0.4 ha per field) in the mean field size. The wheat fields with high optimization efficiency are distributed mainly in the western part of zone IV. In that region, reducing the clay content by 50 $g{\cdot}kg^{-1}$–150 $g{\cdot}kg^{-1}$, adjusting the sand content by -150 $g{\cdot}kg^{-1}$ to $+50$ $g{\cdot}kg^{-1}$, and

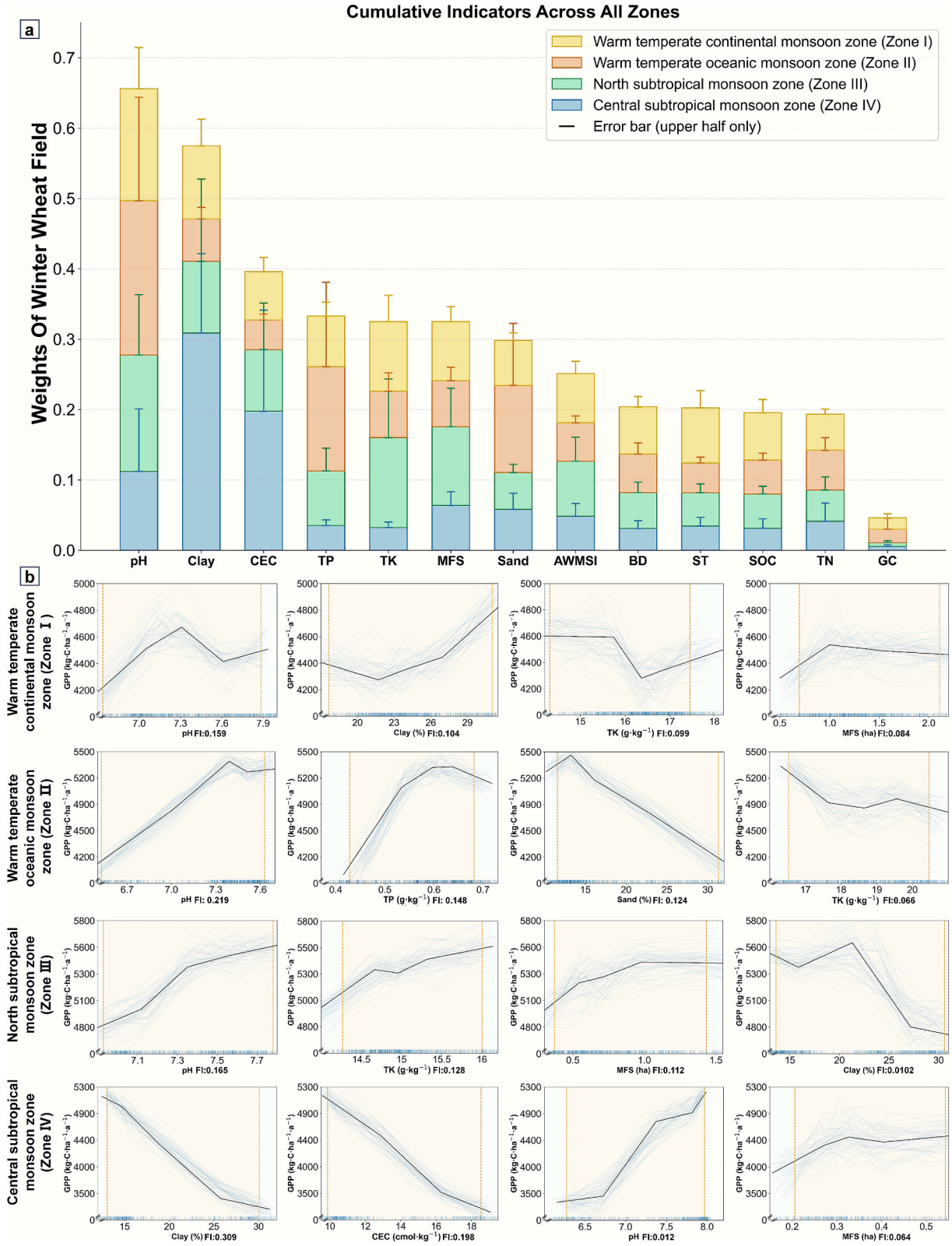

Fig. 5. Farming condition factors' importance and driving patterns on wheat field productivity. In Fig. 5(a), factors are sorted from left to right in descending order according to their cumulative influence intensity in all agricultural climatic homogeneous zones. Fig. 5(b) displays the response of wheat field GPP to changes in the four farming condition factors with the highest importance for each climatic homogeneous zone. FI is an abbreviation of "factor importance". To mitigate the interference of extreme values on the fitted M-plots, the influence ranges of each factor between the 10% and 90% quantiles are highlighted with a light orange background. The full names of each farming condition factor are as follows: BD (soil bulk density, $g{\cdot}cm^{-3}$), GC (gravel content, %), AWMSI (area-weighted mean shape index), MFS (mean field size, ha), pH (soil pH), TN (total nitrogen, $g{\cdot}kg^{-1}$), TK (total potassium, $g{\cdot}kg^{-1}$), TP (total phosphorus, $g{\cdot}kg^{-1}$), SOC (soil organic carbon content, $g{\cdot}kg^{-1}$), ST (soil thickness, mm), CEC (cation exchange capacity, $cmol{\cdot}kg^{-1}$), Sand (sand content, %), and Clay (clay content, %). *The annual influence intensity is shown in Fig. S.5. The response of wheat field productivity to changes in each farming condition factor is shown in Fig. S.6.*

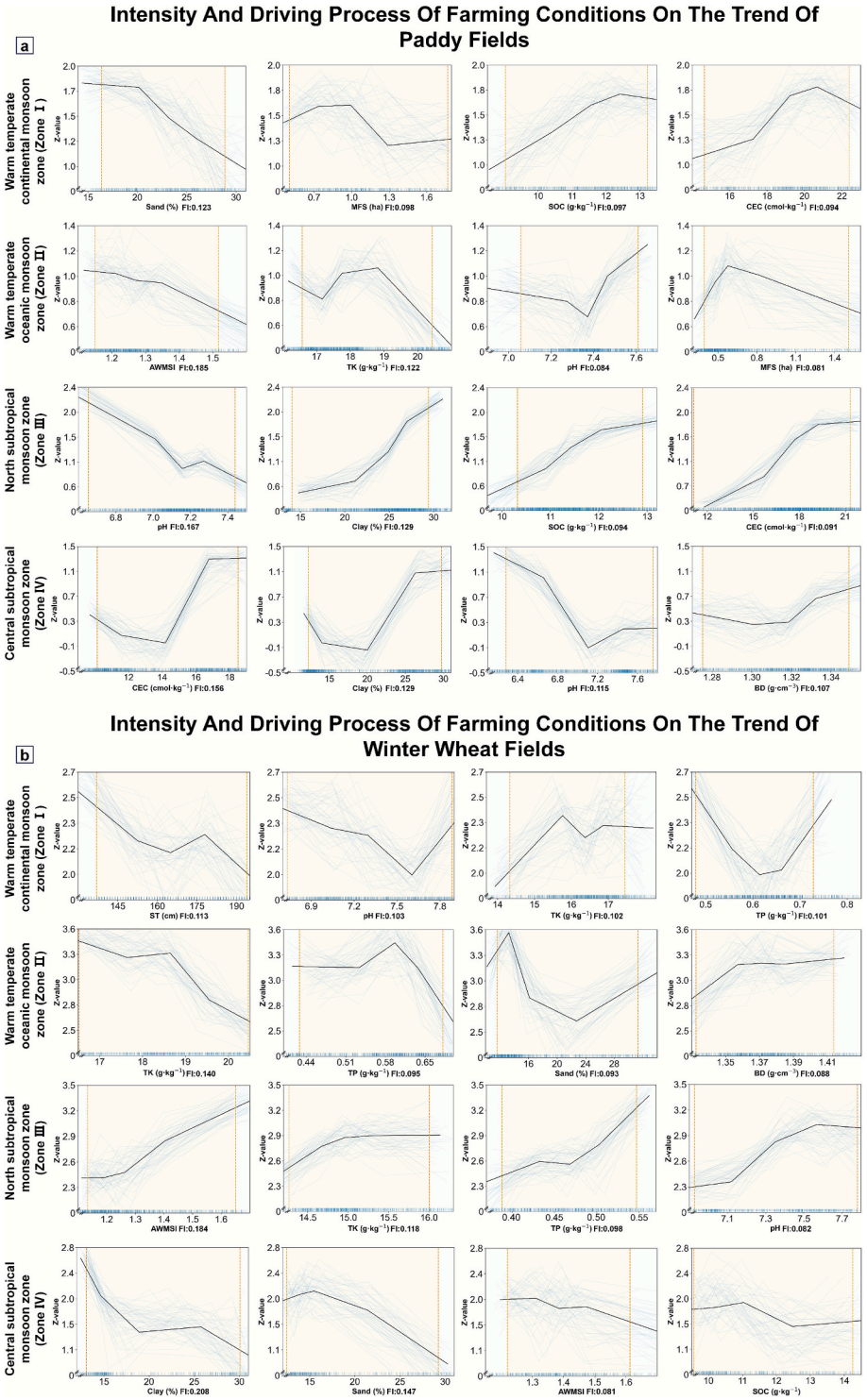

Fig. 6. Intensity and driving process of farming conditions on the trend of paddy field productivity (indicated by the Z-value). Fig. 6a shows the driving processes of the four factors with the highest influence intensity on the trend of paddy field productivity in each homogeneous zone. Fig. 6b shows the driving processes of the four factors with the highest influence intensity on the trend of winter wheat field productivity in each homogeneous zone. 'FI' denotes the factor importance. To mitigate the interference of extreme values on the fitted M-plots, the influence ranges of each factor between the 10% and 90% quantiles are highlighted with a light orange background. The full names of each land surface farming condition factor are as follows: BD (soil bulk density, $g{\cdot}cm^{-3}$), GC (gravel content, %), AWMSI (area-weighted mean shape index), MFS (mean field size, ha), pH (soil pH), TN (total nitrogen, $g{\cdot}kg^{-1}$), TK (total potassium, $g{\cdot}kg^{-1}$), TP (total phosphorus, $g{\cdot}kg^{-1}$), SOC (soil organic carbon content, $g{\cdot}kg^{-1}$), ST (soil thickness, mm), CEC (cation exchange capacity, $cmol{\cdot}kg^{-1}$), Sand (sand content, %), and Clay (clay content, %). *Fig. S.10 shows the response curves of all the factors.*

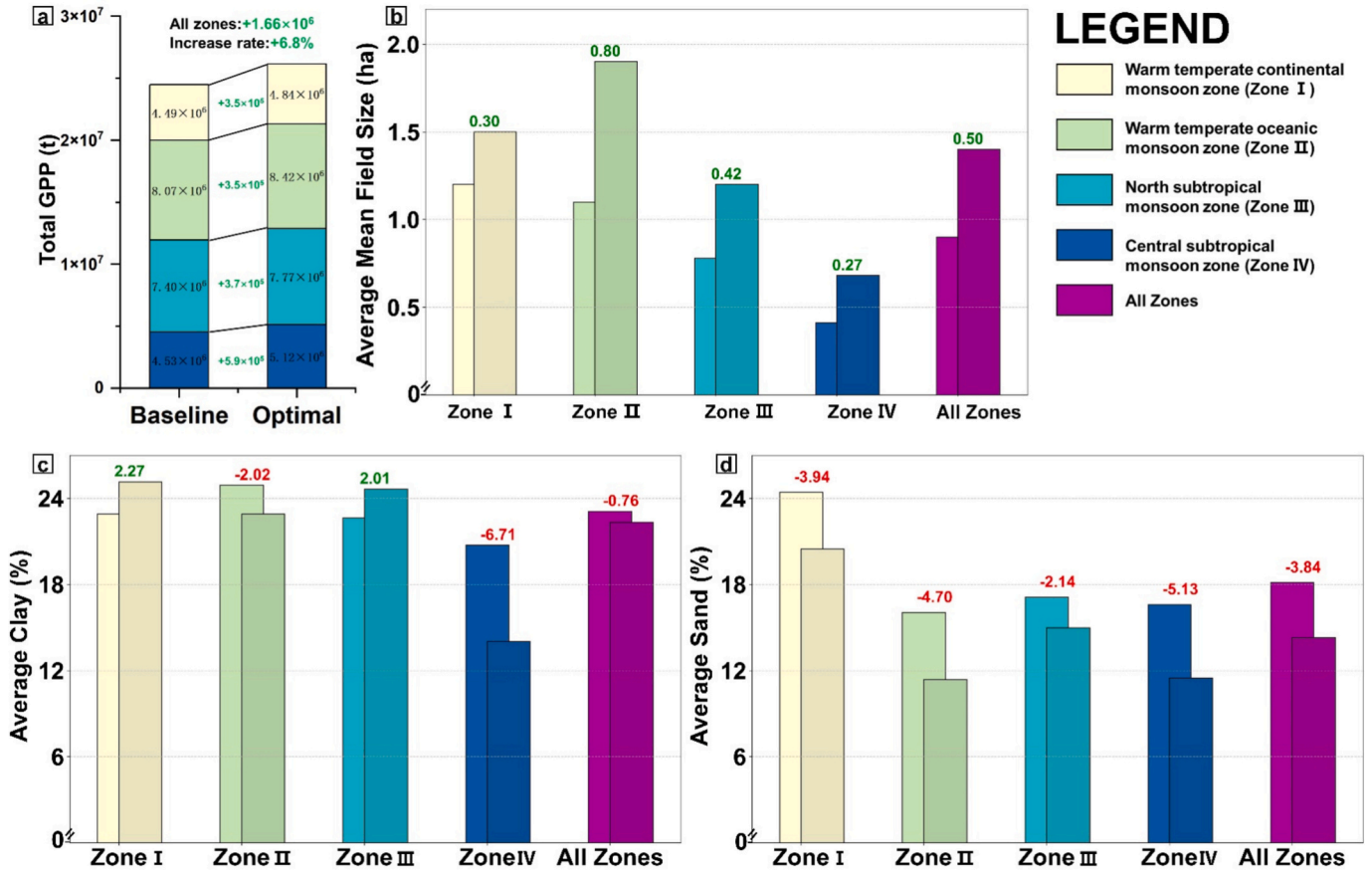

Fig. 7. The potential of optimizing cropland productivity through increasing the mean field size and adjusting the soil clay and sand contents in 1 km resolution grids based datasets of paddy field GPP and wheat field GPP in 2020 has been simulated and used as the baseline scenario. (a) Comparison of the baseline and optimal cropland GPP across the entire study area, with stacked bars coloured corresponding to the agricultural climatic homogeneous zone. (b) Changes in the average mean field size for all the cropland grids in each agricultural climatic homogeneous zone after the optimal GPP objective is achieved. (c) Changes in the clay content for all the cropland grids in each agricultural climatic homogeneous zone after the optimal GPP objective is achieved. (d) Changes in the sand content for all the cropland grids in each agricultural climatic homogeneous zone after the optimal GPP objective is achieved. For each zone, the left bar represents the original value, and the right bar represents the optimized value.

slightly increasing the mean field size can lead to large wheat field GPP gains (> 600 kg·C·ha^{-1}·a^{-1}).

4. Discussion

4.1. Uncertainty analysis

The uncertainty for understanding the influence of farming conditions on cropland productivity can be increased by several factors, including errors in the quantitative characterization of cropland productivity, errors in crop type classification, and the absence of consideration of the influence of cropland input intensity and the cropland infrastructure level.

First, although the reliability of using MODIS GPP data to indicate staple crop yield has been demonstrated (Reeves et al., 2005; Khan et al., 2024), the calculation of GPP inevitably incurs errors due to thin-cloud cover, aerosol variability, and model parameterization, etc. (*see detailed validation of MODIS GPP applicability in Appendix A.16)* Agricultural climatic resources constitute an important driver of crop GPP. The study area was divided into four climatic homogeneous zones to mitigate the influence of spatial variability in agricultural climatic resources. This scheme, however, lacks the ability to address the effects of localized microclimatic differences within each climatic homogeneous zone on crop GPP. Microclimatic deviations are minor in plain regions (e.g., Jiangsu Province). For hilly areas, a more precise delineation of climatic homogeneous zones is needed. Future climate change is expected to exert potential impacts on cropland productivity in Jiangsu Province. Observational and RegCM4.0 evidence indicate that by 2050 Jiangsu will see higher accumulated temperature and solar radiation (Ding et al., 2017). CMIP6 (2015–2100) projects more frequent and intense extreme precipitation under high-emission scenarios across East China, including Jiangsu (Li et al., 2023). In northern Jiangsu (Zones I–II), improved thermal resources may ease current limitations and raise potential yields (Tao and Zhang, 2013). M-plots (Fig. 4b, Fig. 5b) identify soil pH and organic matter as key constraints. Warming intensifies microbial activity and accelerates nitrogen mineralization and nitrification (Dai et al., 2020), further lowering pH and depleting organic matter (Zhao et al., 2013; Miao et al., 2025), thereby reducing cropland productivity. In southern Jiangsu (Zones III, IV), rising extreme rainfall and temperatures will heighten waterlogging risk. Clay content is the dominant constraint, and stronger rainfall can degrade soil structure, increase ponding and internal waterlogging, and favor fungal diseases, amplifying yield losses. Climate-resilient production should prioritize clay soil amelioration, systematic drainage reconstruction via land consolidation, and larger and more contiguous fields to improve mechanization and pest and disease control (Ren et al., 2025).

Local meteorological disasters or crop pest and disease events can exacerbate uncertainties in the quantitative characterization of cropland productivity. For example, the severe floods in 2007 (Wang et al., 2023) and the autumn–winter drought of 2008 (Tao et al., 2009) both resulted in extremely low R^2 (avg. $R^2 = 56.4\%$). To attenuate the influence of localized extreme meteorological events on crop productivity, GPP

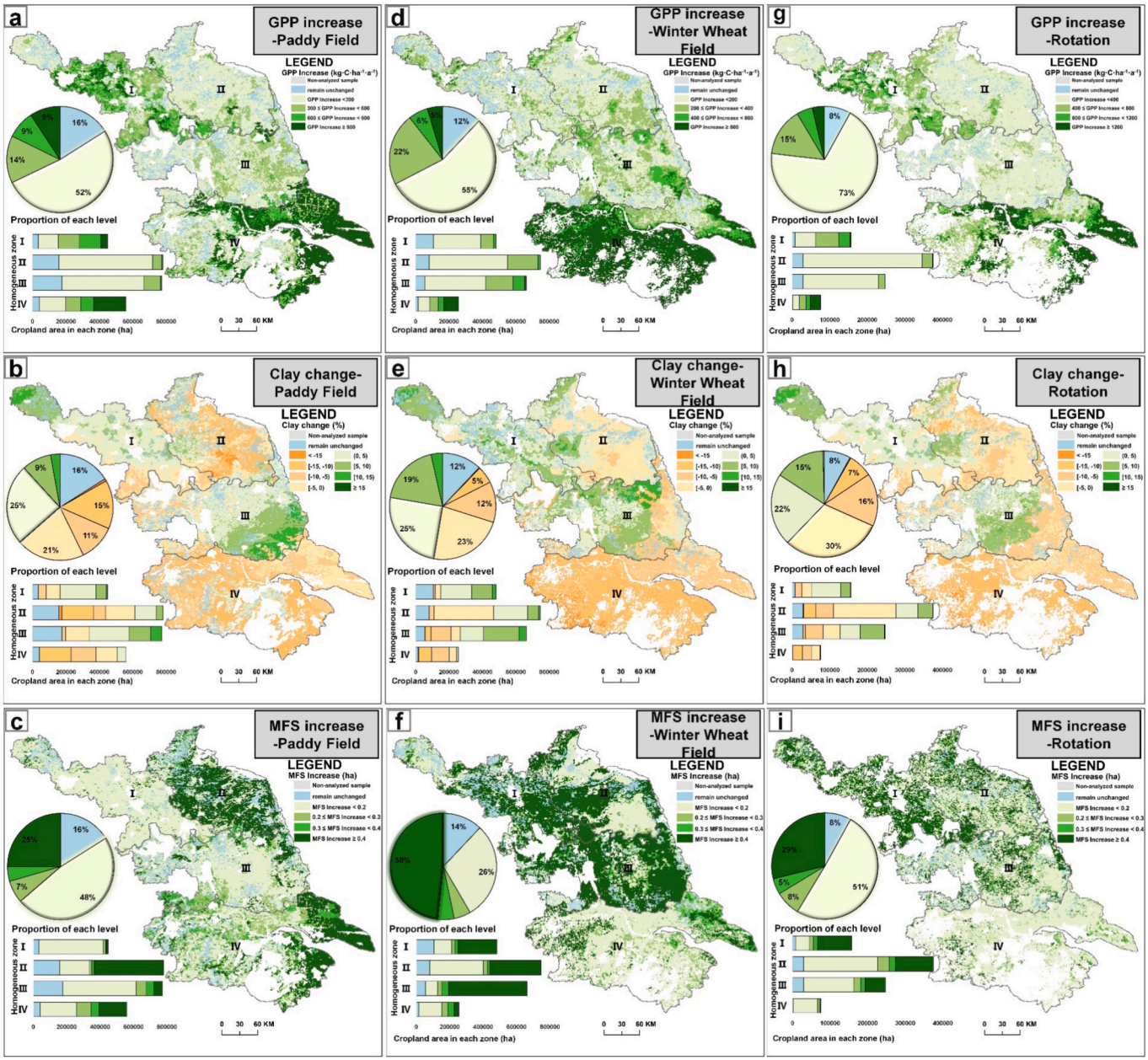

Fig. 8. The 1 km resolution grid-based optimization (optimal scenario) of cropland productivity and the corresponding adjustment strategies for clay content, sand content (*Fig. S.11*) and mean field size. The increases in GPP at each grid caused by the joint optimization of the mean field size and clay content are shown in Fig. 8 a, d and g. *Fig. S.11* shows the spatially simulated annual GPP per unit area (unit: kg C·ha^{-1}·a^{-1}) for paddy, wheat, and paddy-wheat rotation fields as the baseline scenario. The specific adjustment strategies for the clay content and mean field size are shown in Fig. 8 b/e/h/c/f/i. The specific adjustment strategy for the sand content is shown in *Fig. S.11*. Each subplot includes the following: 1. A pie chart showing the proportion of cropland area at each level of the specialty indicator within the given crop type. 2. A horizontal stacked bar chart showing the cumulative area of cropland at each level by agricultural climatic homogeneous zone for the given crop type. The homogeneous zones are labelled I (warm temperate continental monsoon zone), II (warm temperate oceanic monsoon zone), III (north subtropical monsoon zone), and IV (central subtropical monsoon zone).

outlier detection based on a three-standard-deviation filter was executed. Furthermore, climate change and agricultural technological development are the primary drivers of interannual differences in crop GPP. The annual crop GPP from 2001 to 2020 was used as the dependent variable to train the models to test the robustness of the explanatory power of farming conditions on cropland productivity (*Fig. S.3*).

Second, other land use types (e.g., grassland, forestland) that are mixed throughout the 1 km resolution grids will increase the error in crop GPP. The practice of filtering experimental samples by setting a cropland-area threshold has been demonstrated to increase model explanatory power. In comparative tests for paddy fields, when the filtering criterion was set such that cropland comprised more than 20%, 50%, 85%, and 95% of each 1 km grid, the R^2 of the random forest model averaged 0.326, 0.353, 0.438, and 0.608, respectively. Errors in crop-type identification can further increase regression-model uncertainty because of the differences in GPP among crop types. A supervised classification approach based on the dynamic time warping (DTW) model was applied to extract grids predominantly planted with either paddy or wheat from the dataset of the planting areas of three staple crops in China during 2009–2015 (*see detailed information in Appendix A.2*). By increasing the accuracy of crop type identification, the explanatory power of the random forest model for cropland productivity increased

by 9.1% for paddy fields and by 5.8% for wheat fields.

Third, fertilizer, pesticide, and machinery input intensity can affect crop GPP. Cropland input intensity indicators were not considered due to the absence of accurate grid-based data on agricultural intensification, which increases model uncertainty. In regions with generally high levels of agricultural intensification (e.g., Jiangsu Province), the cropland input intensity is sufficient to meet crop growth requirements. The uncertainty introduced by ignoring cropland input intensity is low (Ye et al., 2024a). This view was confirmed by correlation analysis: for each climatic homogeneous zone, the county-level average cropland input intensity and output intensity has weak correlations ($p > 0.05$) (*Fig. S.12*). For regions where cropland input intensity has a high impact on crop yield, it is necessary to introduce multidimensional cropland input intensity indicators as independent variables. Alternatively, spatial differences in cropland input intensity during the homogeneous zone delineation process should be considered. The absence of cropland infrastructure levels (i.e., drainage conditions, irrigation conditions, forest network levels) also increases model uncertainty. Due to the diversity and complexity of infrastructure types, forms, scales and functions, the approaches and methods for observing their characteristics via remote sensing technology have long been limited (Yu et al., 2024a, 2024b). The development of quantitative spatial techniques for assessing cropland infrastructure levels could lead to a more accurate understanding of the mechanisms by which farming conditions influence cropland function. The impact of cropland infrastructure levels on cropland productivity was low (Table 2). This occurred because, as a major agricultural production province, the cropland infrastructure levels in Jiangsu Province generally meet crop growth requirements. For regions with high spatial heterogeneity in cropland infrastructure levels, it is important to use indicators related to cropland infrastructure levels. There is long-term varietal homogenization in Jiangsu Province with a few dominant rice and wheat cultivars such as Nanjing 9108 and Huaimai 33. It results in minor regional differences in crop varieties and a limited influence on productivity assessments. So separate models by variety were not developed (Xu, 2020). Varietal effects are considered when interpreting heterogeneous productivity responses across agricultural climatic homogeneous zones. For instance, the adoption of high-yield, salt-tolerant rice cultivars has enhanced crop resilience in high-pH environments (Hu et al., 2023).

4.2. Explain influence of farming conditions on cropland productivity

Soil texture is the most important factor influencing cropland productivity in Jiangsu Province for both paddy fields and wheat fields. This finding has seldom been reported for cropland productivity in Jiangsu Province (Zhang et al., 2010; Abdul Halim et al., 2018; Hu et al., 2023). Clayey soil can retain abundant levels of moisture and nutrients. An overly clayey soil structure, however, will lead to a reduction in the number of macropores, thereby reducing water and air permeability. In zones I and II, the GPP of both the paddy and wheat fields increased with increasing soil clay content or decreasing sand content. This phenomenon occurred because the precipitation and temperature are both relatively low in these zones, which intensifies crop dependence on the water retention function conferred by the clay content. Excessive sand content leads to poor soil water retention and low soil organic carbon content, which is detrimental to crop growth (Xu et al., 2017). For paddy fields in zone II, when the clay content exceeded 25%, the paddy field GPP decreased with further increases in the clay content. This occurred because most paddy fields with clay contents above 25% simultaneously had high sand contents (approximately 20%) in zone II (*Fig. S.7*). The negative effect of increasing the sand content on the paddy field GPP (influence intensity = 0.13) exceeded the positive effect of increasing the clay content (influence intensity = 0.08) (Fig. 4). In zones III and IV, where the temperature and precipitation are relatively high, increases in the clay content restricted soil drainage and aeration, leading to declines in the wheat field GPP. In particular, in the subtropical monsoon zone (i.e., zone IV), the clay content was the primary limiting factor for wheat field GPP. The reason is high clay content restricts soil aeration and water drainage, leading to oxygen deficiency in the root zone. This condition inhibits root respiration and nutrient uptake, causing severe energy shortage (Colmer and Greenway, 2011) and cell death in the root apical meristem (Herzog et al., 2016). Hypoxia also suppresses nitrate reductase activity and reduces nitrogen assimilation, resulting in poor grain quality (Zhao et al., 2004). Moreover, the high soil moisture associated with clayey soils promotes the proliferation of soil-borne pathogens such as Fusarium and Pythium, increasing susceptibility to root rot and other fungal diseases. Field observations have shown that Zone IV in Jiangsu is one of the regions most severely affected by Fusarium head blight (Feng et al., 1995), which further constrains wheat GPP under such conditions. Increases in sand content also corresponded to declines in wheat field GPP, which indicates that increases in silt content are the top priority for enhancing GPP. For paddy fields in zones III and IV, increases in clay content within the 20–30% range still corresponded to increases in cropland GPP. This occurred because the rhizosphere processes in paddy fields can adapt to anaerobic conditions (Wei et al., 2022), and the increase in water retention function resulting from increased clay content benefits rice growth. In a field experiment conducted on paddy fields in southern Jiangsu Province, Zhang (1988) noted that when the soil clay content approached 20%, the nitrogen supply capacity, soil organic carbon content, and total soil nitrogen content declined rapidly to extremely low levels, resulting in reduced paddy yields (Fig. 4b; *Fig. S.6*). Paddy field samples with soil silt contents near 20% are concentrated in the cities of Yancheng, Taizhou, and Yangzhou (Fig. 9a, b).

Soil pH was another primary factor influencing cropland productivity for both paddy fields and wheat fields. The driving pattern of soil pH on the GPP of wheat fields was approximately consistent in each zone: within the pH range of 6.3–7.3, increases in pH drove increases in GPP. Especially in zone IV, increases in soil pH still increased the wheat field GPP even at pH values above 7.5. This occurred because a high pH indicates strong oxidation of the soil, which depends on high soil aeration. This view is supported by the correlation analysis among farming conditions (*Fig. S.13*): in zone III and IV, the pH and clay content were strongly negatively correlated (Pearson's $r < -0.8$, $p < 0.001$). The soils under wheat cultivation in Jiangsu are largely alluvial soils, which have strong acid-buffering capacity and high fertility (Wang et al., 2008). The breeding of salt-alkali–tolerant wheat varieties has effectively increased the resistance of wheat to high pH (Hu et al., 2023). Increases in soil pH generally corresponded to decreases in paddy field GPP. This occurred because a low pH indicates a strong soil reduction reaction, which facilitates the uptake of micronutrients by rice (Abdul Halim et al., 2018). One exception occurred in zone IV, where increases in soil pH within the 7.3–8.0 range increased paddy field GPP. This occurred because, in local areas with pH values above 7.3, conventional rice was replaced by hybrid rice varieties that possess relatively strong alkali tolerance and high GPP. In zone II, paddy fields with pH values within 7.25–7.55 are distributed mainly in low-lying areas severely affected by waterlogging and drought and with weak agricultural infrastructure (Fig. 9c). This explains why the paddy field GPP response curve has an anomalous "U"-shaped trough in response to pH (Fig. 4).

Soil organic carbon content is widely recognized as an important

Table 2
Results of the factor theory detector for cultivated land artificial input.

Crop type	Crop land Infrastructure Conditions	Mean *q* value	Mean *p* value
Paddy	Degree of forest network	0.020	0.997
	Agricultural mechanization level	0.009	1
	Drainage condition	0.010	0.999
Winter wheat	Degree of forest network	0.028	0.239
	Agricultural mechanization level	0.012	0.995
	Drainage condition	0.010	0.843

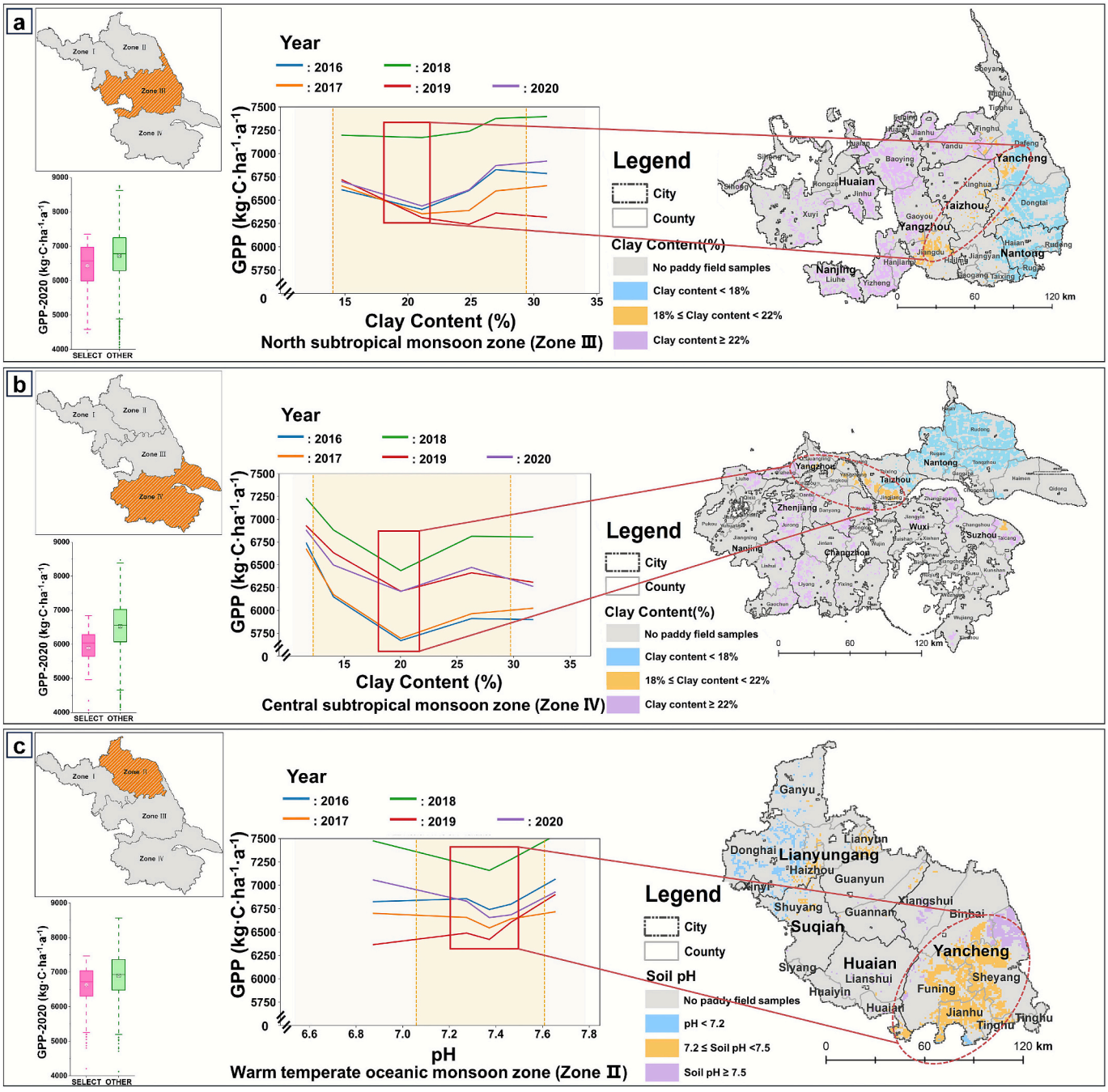

Fig. 9. Interpretation of the mutational curve segments of the clay content (zones III and IV) and soil pH (zone II) in the M-plot results for paddy fields. In each subplot, the bottom-left boxplot compares the GPP of the region highlighted by the red circle in 2020 to that of other areas. The central line chart depicts the response of GPP to changes in clay content (a, b) and soil pH (c) in specific zones from 2016 to 2020. The sections highlighted with red boxes in the line chart indicate mutational curve segments. The main distribution areas corresponding to paddy fields whose soil clay content or pH values belong to the mutational curve segments are marked with red boxes and orange renderings on the map. (For interpretation of the references to colour in this figure legend, the reader is referred to the web version of this article.)

indicator affecting cropland productivity (Lal, 2006; Pan et al., 2009). An increase in soil organic carbon content can increase cropland productivity by increasing available water capacity, strengthening nutrient supply and soil structure. For example, Lal noted that every 1 $Mg{\cdot}ha^{-1}$ increase in the soil organic carbon pool could increase wheat yield by 20–70 $kg{\cdot}ha^{-1}$, paddy yield by 10–50 $kg{\cdot}ha^{-1}$, and maize yield by 30–300 $kg{\cdot}ha^{-1}$. Increases in soil organic carbon had an important influence (intensity = 0.27) on increasing the paddy field GPP only in zone I. This result occurred because the soil organic carbon in Jiangsu Province croplands is generally at a medium-to-low level (below 1.5%), and soil texture plays a more important role than organic carbon and bulk density in determining soil water retention, nutrient-holding capacity, and aeration. Within the 8.9–12 $g{\cdot}kg^{-1}$ range in zone I, an average 1 $g{\cdot}kg^{-1}$ increase in soil organic carbon corresponded to a 320 $kg{\cdot}C{\cdot}ha^{-1}{\cdot}a^{-1}$ increase in paddy field GPP.

The cation exchange capacity, which indicates the soil nutrient-holding capacity, was strongly correlated with the clay content (Pearson's $r = 0.87$, $p < 0.001$). The response curve of GPP to changes in the cation exchange capacity was similar to that for the clay content (*Fig. S.6*).

A sufficient potassium and phosphorus supply provides important support for increasing crop drought, cold resistance, and root and fruit development. Excessive potassium and phosphorus, however, can reduce nutrient uptake and exacerbate soil acidification and compaction. M-plot models identified the inflection points at which increases in soil total potassium and total phosphorus turn to reduce cropland GPP. Total potassium becomes excessive when it exceeds 16 $g{\cdot}kg^{-1}$, and further increases corresponded to declines in the cropland GPP. The inflection point for total phosphorus excessive status lies between 0.5 and 0.6 $g{\cdot}kg^{-1}$.

As a major grain-producing province located in the plain area, Jiangsu Province has the highest contiguous distribution of cropland in China (Ye et al., 2024b). Under the household contract responsibility system, however, originally contiguous cropland has been subdivided into numerous fragmented plots and allocated to different farm households. This process has made Jiangsu Province one of the provinces with the highest degree of field fragmentation (Ye et al., 2024b; Zhang et al., 2024). Since field fragmentation is generally high, reducing fragmentation to expand farm size will result in little increase in cropland GPP. The mean wheat field size is primarily distributed in the 0.25–1.0 ha per field range. In this range, increases in the mean field size drive increases in the cropland GPP. In the range above 1.0 ha per field, increases in the mean field size correspond to a steady or even reduced GPP. This phenomenon occurs is because the smallholder-dominated farming system lacks practical experience in scaling-up operations and sufficient agricultural machinery support to adapt to larger field sizes. Compared with wheat fields, paddy fields are generally small, rely on manual fine tillage, and are severely constrained by land levelling techniques and farm machinery. In the range above 0.5 ha per field, increases in the mean field size will correspond to reductions in paddy field GPP. Similarly, a field survey-based study in zone IV noted that field size had little effect on paddy yield (Lv et al., 2014).

4.3. *Strategies for increasing cropland productivity: From science to policy*

Adjusting soil texture and consolidating fragmented fields for the reclamation of low- and medium-yield croplands have long been key components of Chinese farmland development policy. The General Standards for High-Standard Farmland Construction in China explicitly request soil amelioration through local measures such as sand mixing, clay mixing, soil replacement, and organic matter addition to address excessively sandy or clayey soils (Chen and Peng, 2024). The 2025 No. 1 Central Document (State Council, Opinions on Further Deepening Rural Reform and Advancing Rural Revitalization in an All-round Way) also emphasizes mitigating cropland fragmentation. In the provincial guidelines for high-standard farmland construction, however, most provinces did not provide implementation suggestions for soil texture adjustment and fragmented cropland rationalization. In the study case of Jiangsu Province, we found that adjusting soil texture has a high-intensity effect on increasing cropland productivity. Based on 1 km grids, the potential of raising cropland productivity by adjusting soil texture and reducing farmland fragmentation have been simulated.

For paddy fields and wheat fields, adjusting the plough layer soil texture and increasing the mean field size can increase the annual GPP by 1.65×10^6 t, representing 6.8% of the total annual GPP (Figs. 7, 8). Paddy fields contribute 1.02×10^6 t and wheat fields contribute 0.63×10^6 t. In high-standard farmland construction projects or medium-to-low-yield field renovation projects, cropland productivity can be further increased by implementing soil amelioration measures, specifically adjusting the clay–sand–silt ratio in the plough layer, alongside infrastructure construction. An increase in GPP per unit area was correlated with a decrease in the baseline GPP ($r = -0.29$ for paddy fields; $r = -0.62$ for wheat fields; $r = -0.44$ for rotation fields, $p < 0.001$) (*Fig. S.14*). These findings indicate that soil texture improvement projects are most suitable for wheat fields or paddy-wheat rotation fields with low cropland productivity. Zone IV had the highest applicability: in its eastern part, the paddy field GPP increased by more than 900 $kg{\cdot}C{\cdot}ha^{-1}{\cdot}a^{-1}$; in its western part, the wheat field GPP increased by more than 600 $kg{\cdot}C{\cdot}ha^{-1}{\cdot}a^{-1}$. To achieve these targets in zone IV, the clay and sand contents in most paddy fields should be reduced by 0–100 $g{\cdot}kg^{-1}$, and those in most wheat fields should be reduced by 50–150 $g{\cdot}kg^{-1}$ and 0–50 $g{\cdot}kg^{-1}$, respectively. In some grids, soil-texture adjustment is inadvisable because the optimization directions for clay or sand content conflict between paddy fields and wheat fields.

Due to limitations in the current provision of agricultural machinery and equipment, field fragmentation was detected to have a low influence intensity on cropland productivity. For grids with mean field sizes exceeding 1.0 ha and 0.5 ha per field (Fig. 4b, Fig. 5b), increases in the mean field size corresponded to decreases in the cropland productivity of both wheat fields and paddy fields. This is not evidence that increasing the mean field size should be disregarded as a strategy for increasing cropland productivity. A study based on surveys of over 40,000 farm households proposed that by consolidating 86% of Chinese farmland to establish a large-scale farming regime with an average field size greater than 16 ha, the total nitrogen input could be reduced by 24%, nitrogen use efficiency could be increased by 18%, labour demand could be reduced by 39%, and labour income could double (Duan et al., 2021). For cropland planted solely with wheat, the core challenge is how to surpass the mean field size threshold of 1.0 ha per field and construct large-scale cultivation. When facilitating land transfer and consolidation, local government departments should attach importance to the matching of agricultural machinery and equipment for cultivation, raise subsidy standards for farm machinery purchases, and stimulate economies of scale in cropland management. For croplands planted solely with paddy crops, relevant standards need to be formulated to control the size of individual plots in high-standard farmland construction projects or dryland-to-paddy conversion projects. Simultaneously, the development of farming cooperatives should be encouraged to prioritize the consolidation of highly fragmented plots, forming contiguous paddy fields with standard areas of 0.3–0.5 ha per field. For paddy–wheat rotation cropland, the key task will be to explore how to ensure simultaneous increases in paddy field GPP and wheat field GPP when the mean field size is increased to 1.0 ha per field. Practical experiences from Japan and the plains in Northeast China can guide this effort. In the 1990s, 55% of Japanese paddy fields were consolidated to 0.3 ha per field (Sato, 2001). The Japanese government then offered further subsidies to increase the consolidation of these 0.3 ha fields into large-scale fields exceeding 1.0 ha in area (He et al., 2022). In the Sanjiang Plain of Northeast China, paddy fields exceeding 1.0 ha are also present (Ye et al., 2024b).

Simulation results show that simultaneous adjustments to MFS and soil texture (clay and sand) produce a synergistic effect. Even for grids with initially large MFS values (beyond 0.5 ha for paddy and 1.0 ha for winter wheat), the optimization scenario still results in higher GPP. 84% of paddy-only, 88% of winter wheat-only, and 92% of paddy–wheat rotation grids achieved GPP increases under the scenario (Fig. 8a, d, g), demonstrating that synchronous adjustment of MFS and soil texture is an effective strategy to enhance cropland productivity.

The proposed optimization strategies are economically feasible because of existing national and provincial investments. The National Plan for High-Standard Farmland Construction (2021−2030) estimates an average input of ~45,000 CNY per ha, with additional subsidies provided by provincial governments. These funds can cover typical land consolidation costs of ~24,000 CNY per ha in China (Duan et al., 2021; Chen and Peng, 2024; Feng et al., 2024). Provincial technical guidelines provide explicit operational standards for soil-texture modification. For example, the High-Standard Farmland Construction Guidelines of Hunan Province specify that improving overly sandy or overly clayey soils through sand mixing or clay mixing typically enables adjustments of approximately 100 $g{\cdot}kg^{-1}$ in soil texture composition. In the study area, the optimal GPP simulations required only 50–70 $g{\cdot}kg^{-1}$ changes in clay or sand content on average (Fig. 7), with only 17.73% of grids exceeding 100 $g{\cdot}kg^{-1}$ and 4.65% exceeding 150 $g{\cdot}kg^{-1}$. These results

indicate that for the vast majority of grids in Jiangsu Province, the simulated soil-texture adjustments fall well within the feasible range defined by current High-Standard Farmland Construction practices. Regarding increasing mean field size, field consolidation is likewise financially supported through local subsidies (~3000 CNY per ha), enabling more efficient land management and productivity gains (Zhang et al., 2020).

Croplands with excessive total potassium (> 16 g·kg^{-1}) and excessive total phosphorus (> 0.6 g·kg^{-1}) are located primarily in zones I and II (*Fig. S.15, S.16*). In these zones, reducing phosphorus and potassium fertilizer inputs or adopting other measures to decrease total phosphorus and potassium contents could help increase cropland productivity. In most areas of zones III and IV, the total potassium and total phosphorus levels are low, suggesting that modest increases in phosphorus and potassium fertilizer inputs are appropriate.

When applying our modelling framework to other study regions, several considerations should be taken into account to ensure its validity and robustness. First, data availability must be ensured, as the framework relies not only on reliable GPP products such as MOD17A2H but also on locally accessible datasets describing soil physicochemical properties, cropland distribution, and crop types. Second, delineating agricultural climatic homogeneous zones is essential to minimize the effects of spatial heterogeneity in climatic resources; in regions with complex terrain such as hilly or mountainous areas, a finer climatic zoning approach is recommended. Third, the framework should be adapted to the dominant cropping systems in the target region—for example, separate models should be developed for maize–soybean rotation, single-season rice, or cash crops. Finally, the selection of farming condition factors should be tailored to regional agricultural contexts; in areas characterized by low input intensity, management and input indicators should be incorporated explicitly, and necessary pre-analysis steps such as multicollinearity diagnosis should be conducted prior to model construction.

5. Conclusions

A modelling framework to analyse the influence mechanisms of land surface farming conditions on cropland productivity in scenarios lacking high-precision crop yield data was proposed and applied in a typical grain-producing province in the plain region of China. First, farming conditions explained > 60% of the spatial variability in paddy field GPP and > 65% of the spatial variability in wheat field GPP. Soil texture and pH were the primary factors affecting the GPP of rice and wheat. In most scenarios, decreases in sand content and increases in clay content generally increased the GPP of paddy fields. In the 10–20% range, however, increases in clay led to a rapid decline in the soil nitrogen supply, thereby decreasing paddy field GPP. Climate conditions influenced the preference of wheat for soil water retention and drainage-permeability, resulting in an increase in wheat GPP in northern regions and a decrease in clay content in southern regions. An increase in pH caused a decrease in paddy field GPP and an increase in wheat field GPP. When conventional rice was replaced with hybrid rice, increases in pH increased the GPP of paddy fields. In the range of < 1.0 ha per field or < 0.5 ha per field, the GPP of wheat fields or paddy fields increased as the mean field size increased.

Second, by increasing the mean field size and adjusting the soil clay and sand contents, the total GPP of paddy and wheat fields increased by 6.8%. Paddy fields and paddy-wheat rotation fields in zone I and the eastern region of zone IV had high optimization efficiencies. In these areas, small adjustments (− 50 g·kg^{-1} to +50 g·kg^{-1}) to the soil clay and sand contents generally induced GPP increases exceeding 600 kg·C·ha^{-1}·a^{-1} for paddy fields and 800 kg·C·ha^{-1}·a^{-1} for paddy–wheat rotation fields. High-efficiency wheat fields are primarily distributed in the region of western zone IV. In that region, the wheat field GPP was greatly increased (> 600 kg·C·ha^{-1}·a^{-1}) by reducing the clay content by 50 g·kg^{-1}–150 g·kg^{-1}, adjusting the sand content by −150 g·kg^{-1} to +50 g·kg^{-1}, and slightly increasing the mean field size.

In the future, large-scale studies need to further integrate the effects of spatial heterogeneity in agricultural intensification and cropland infrastructure on cropland productivity and remove samples where severe agricultural disasters occur from the analysis. In zone IV, high-standard farmland construction projects or medium- to low-yield field renovation initiatives should be accompanied by soil texture adjustment measures to reduce clay and sand contents. This framework can provide technical support for increasing farming conditions in low- to medium-yield cropland renovation projects and future national arable land quality assessment projects in China.

CRediT authorship contribution statement

Xiaoyang Han: Writing – original draft, Visualization, Methodology, Data curation. **Changqing Song:** Supervision, Project administration, Funding acquisition, Conceptualization. **Leina Zhang:** Resources, Project administration. **Peichao Gao:** Funding acquisition, Formal analysis. **Sijing Ye:** Writing – review & editing, Writing – original draft, Visualization, Methodology, Formal analysis, Conceptualization. **Yakov Kuzyakov:** Writing – review & editing, Formal analysis.

Declaration of competing interest

None.

Acknowledgements

This research was funded by National Natural Science Foundation of China [Grant No. 42571308, 42171250, 42230106, 42271418]. We would like to thank the high-performance computing support from the Center for Geodata and Analysis, Faculty of Geographical Science, Beijing Normal University, and the RUDN University Strategic Academic Leadership Program.

Appendix A. Supplementary data

Supplementary data to this article can be found online at https://doi.org/10.1016/j.agsy.2026.104635.

Data availability

Data will be made available on request.

References

Abdul Halim, N., Abdullah, R., Karsani, S., et al., 2018. Influence of soil amendments on the growth and yield of rice in acidic soil. Agronomy 8 (9), 165.
Bolton, D., Friedl, M., 2013. Forecasting crop yield using remotely sensed vegetation indices and crop phenology metrics. Agric. For. Meteorol. 173, 74–84.
Chen, L., Peng, J., 2024. Effects of China's high-standard farmland construction policy on grain production capacity and its mechanisms. Resour. Sci. 46 (01), 145–159 (in Chinese with English abstract).
Chen, J., Ban, Y., Li, S., 2014. China: open access to earth land-cover map. Nature 514 (7523).
Chen, J., Chen, J., Liao, A., et al., 2015. Global land cover mapping at 30 m resolution: a POK-based operational approach. ISPRS J. Photogramm. Remote Sens. 103, 7–27.
Colmer, T.D., Greenway, H., 2011. Ion transport in seminal and adventitious roots of cereals during O_2 deficiency. J. Exp. Bot. 62 (1), 39–57.
Dai, Z., Xu, X., Zhu, J., et al., 2020. Elevated temperature shifts soil N cycling from microbial immobilization to enhanced mineralization, nitrification and denitrification across global terrestrial ecosystems. Glob. Chang. Biol. 26 (9), 5267–5276.
Deines, J., Patel, R., Liang, S., et al., 2021. A million kernels of truth: insights into scalable satellite maize yield mapping and yield gap analysis from an extensive ground dataset in the US Corn Belt. Remote Sens. Environ. 253, 112174.
Ding, C., Shen, S., Tao, S., 2017. Agricultural climatic resources and future scenario projections in Jiangsu Province. Acta Agric. Jiangsu 33 (6), 1309–1315 (in Chinese with English abstract).
Dong, J., Fu, Y., Wang, J., et al., 2020. Early season mapping of winter wheat in China based on landsat and sentinel images. Earth Syst. Sci. Data Discuss. 2020, 1–26.

Doran, J., Parkin, T., 1994. Defining and assessing soil quality. In: Defining Soil Quality for a Sustainable Environment, 35, pp. 1–21.
Du, B., Ye, S., Gao, P., et al., 2024. Analyzing spatial patterns and driving factors of cropland change in China's National Protected Areas for sustainable management. Sci. Total Environ. 912, 169102.
Duan, J., Ren, C., Wang, S., et al., 2021. Consolidation of agricultural land can contribute to agricultural sustainability in China. Nat. Food 2 (12), 1014–1022.
Duflot, R., San-Cristobal, M., Andrieu, E., et al., 2022. Farming intensity indirectly reduces crop yield through negative effects on agrobiodiversity and key ecological functions. Agric. Ecosyst. Environ. 326, 107810.
Fang, H., Liang, S., Hoogenboom, G., et al., 2008. Corn-yield estimation through assimilation of remotely sensed data into the CSM-CERES-maize model. Int. J. Remote Sens. 29 (10), 3011–3032.
Fathizad, H., Ardakani, M., Heung, B., et al., 2020. Spatio-temporal dynamic of soil quality in the central Iranian desert modeled with machine learning and digital soil assessment techniques. Ecol. Indic. 118, 106736.
Feng, C., Zhang, G., Chen, Z., 1995. Climatic regionalization of wheat scab distribution in Jiangsu Province. Acta Phytopathol. Sin. 2, 111–115 (in Chinese).
Feng, J., Zhang, X., Lin, W., 2024. The impacts of high-standard farmland construction on cultivated land improvement in China. Sustainability 16 (16), 6970.
Foley, J., Ramankutty, N., Brauman, K., et al., 2011. Solutions for a cultivated planet. Nature 478 (7369), 337–342.
Gao, P., Gao, Y., Zhang, X., et al., 2023. CLUMondo-BNU for simulating land system changes based on many-to-many demand–supply relationships with adaptive conversion orders. Sci. Rep. 13 (1), 5559.
Gong, H., Zhao, Z., Chang, L., et al., 2022. Spatiotemporal patterns in and key influences on cultivated-land multi-functionality in Northeast China's black-soil region. Land 11 (7), 1101.
Guillaume, T., Maranguit, D., Murtilaksono, K., et al., 2016. Sensitivity and resistance of soil fertility indicators to land-use changes: new concept and examples from conversion of Indonesian rainforest to plantations. Ecol. Indic. 67, 49–57. https://doi.org/10.1016/j.ecolind.2016.02.039.
Halvorson, A., Wienhold, B., Black, A., 2002. Tillage, nitrogen, and cropping system effects on soil carbon sequestration. Soil Sci. Soc. Am. J. 66 (3), 906–912.
He, J., Zhou, X., Matsui, T., et al., 2022. Critical reevaluation of an efficient sampling design for assessing soil properties using bootstrap sampling and geostatistical analysis in Japanese large-scale Paddy fields. Soil Sci. Plant Nutr. 68 (5–6), 536–546.
Herzog, M., Striker, G.G., Colmer, T.D., et al., 2016. Mechanisms of waterlogging tolerance in wheat: a review of root and shoot physiology. Plant Cell Environ. 39 (5), 1068–1086.
Hu, P., Tu, F., Li, S., et al., 2023. Low-cd wheat varieties and soil cd safety thresholds for local soil health management in South Jiangsu province, East China. Agric. Ecosyst. Environ. 341, 108211.
Hu, P., Zheng, B., Chen, Q., et al., 2024. Estimating aboveground biomass dynamics of wheat at small spatial scale by integrating crop growth and radiative transfer models with satellite remote sensing data. Remote Sens. Environ. 311, 114277.
Huang, J., Tian, L., Liang, S., et al., 2015. Improving winter wheat yield estimation by assimilation of the leaf area index from Landsat TM and MODIS data into the WOFOST model. Agric. For. Meteorol. 204, 106–121.
Huang, J., Becker-Reshef, I., Huang, H., et al., 2019. Assimilation of remote sensing into crop growth models: current status and perspectives. Agric. For. Meteorol. 276–277, 107609.
Huang, H., Huang, J., Wu, Y., et al., 2023. The improved winter wheat yield estimation by assimilating GLASS LAI into a crop growth model with the proposed Bayesian posterior-based ensemble Kalman filter. IEEE Trans. Geosci. Remote Sens. 61, 1–18.
Jiangsu Provincial Bureau of Statistics, 2023. Jiangsu Statistical Yearbook 2023. China Statistics Press, Beijing (in Chinese).
Khan, S., Li, D., Maimaitijiang, M., 2024. Using gross primary production data and deep transfer learning for crop yield prediction in the US Corn Belt. Int. J. Appl. Earth Obs. Geoinf. 131, 103965.
Kuzyakov, Y., Gunina, A., Zamanian, K., et al., 2020. New approaches for evaluation of soil health, sensitivity and resistance to degradation. Front. Agric. Sci. Eng. 7 (3), 282–288. https://doi.org/10.15302/J-FASE-2020338.
Lal, R., 2006. Enhancing crop yields in the developing countries through restoration of the soil organic carbon Pool in agricultural lands. Land Degrad. Dev. 17, 197–209.
Lal, R., 2018. Digging deeper: a holistic perspective of factors affecting soil organic carbon sequestration in agroecosystems. Glob. Chang. Biol. 24 (8), 3285–3301.
Larson, W., Pierce, F., 1991. Conservation and Enhancement of Soil Quality, 175–203.
Li, H., Luan, C., Xia, X., et al., 2023. Projection of future extreme precipitation scenarios in mainland China based on CMIP6 climate models. Water Resourc. Hydropower Eng. 54 (8), 16–29.
Liu, C., Song, C., Ye, S., et al., 2023. Estimate provincial-level effectiveness of the arable land requisition-compensation balance policy in mainland China in the last 20 years. Land Use Policy 131, 106733.
Liu, F., Zhang, G., Song, X., et al., 2020a. High-resolution and three-dimensional mapping of soil texture of China. Geoderma 361, 114061.
Liu, F., Wu, H., Zhao, Y., et al., 2022. Mapping high resolution national soil information grids of China. Sci. Bull. 67 (3), 328–340.
Liu, L., Zhou, D., Chang, X., et al., 2020b. A new grading system for evaluating China's cultivated land quality. Land Degrad. Dev. 31 (12), 1482–1501.
Liu, S., Fu, B., Liu, G., et al., 2006. Research review of quantitative evaluation of soil quality in China. Chin. J. Soil Sci. 01, 137–143 (in Chinese with English abstract).
Lv, T., Ji, Y., Yi, Z., 2014. Plot economies of scale in rice production: based on the investigation and analysis of Jitan in Changzhou, Jiangsu province. J. Agrotechn. Econ. 02, 68–75 (in Chinese).
Mann, H., 1945. Nonparametric test against trend. Econometrica 13 (3), 245–259.
Mei, Q., Zhang, Z., Luo, Y., et al., 2023. A dataset of the planting areas of three staple crops with a spatial resolution of 1 km in China during 2009–2015. China Sci. Data 8 (3) (in Chinese with English abstract).
Miao, S., Tang, Y., Li, H., et al., 2025. Simulation of the effects of extreme rainfall and biochar on nitrogen loss in winter wheat fields using the DNDC model. J. Agro-Environ. Sci. 1–13.
Obade, V., Lal, R., 2016. A standardized soil quality index for diverse field conditions. Sci. Total Environ. 541, 424–434.
Office of the Third National Land Survey Leading Group of the State Council, Ministry of Natural Resources, National Bureau of Statistics, 2021. Major data bulletin of the third National Land Survey. Nat. Land Resourc. Informa. 17, 7–8 (in Chinese).
Pan, G., Zhou, P., Li, Z., et al., 2009. Combined inorganic/organic fertilization enhances N efficiency and increases Rice productivity through organic carbon accumulation in a Rice Paddy from the Tai Lake region, China. Agric. Ecosyst. Environ. 131, 274–280.
Pan, B., Zheng, Y., Shen, R., et al., 2021. High resolution distribution dataset of double-season Paddy Rice in China. Remote Sens. 13, 4609.
Paul, G., Saha, S., Ghosh, K., 2020. Assessing the soil quality of Bansloi river basin, eastern India using soil-quality indices (SQIs) and random Forest machine learning technique. Ecol. Indic. 118, 106804.
Paustian, K., Andren, O., Janzen, H., et al., 1997. Agricultural soils as a sink to mitigate CO_2 emissions. Soil Use Manag. 13, 230–244.
Peng, S., Ding, Y., Liu, W., et al., 2019. 1 km monthly temperature and precipitation dataset for China from 1901 to 2017. Earth Syst. Sci. Data 11, 1931–1946.
Reeves, M., Zhao, M., Running, S., 2005. Usefulness and limits of MODIS GPP for estimating wheat yield. Int. J. Remote Sens. 26 (7), 1403–1421.
Ren, S., Song, C., Ye, S., et al., 2022. The spatiotemporal variation in heavy metals in China's farmland soil over the past 20 years: a meta-analysis. Sci. Total Environ. 806, 150322.
Ren, S., Song, C., Ye, S., et al., 2023. Land use evaluation considering soil properties and agricultural infrastructure in Black soil region. Land Degrad. Dev. 34 (17), 5373–5388.
Ren, S., Ye, S., Zhang, L., et al., 2025. Reducing cropland fragmentation may not be universally beneficial at increasing land use efficiency: evidence from multiscale spatial analysis of Huang-Huai-Hai region, China. Land Use Policy 159, 107806.
Rinot, O., Levy, G., Steinberger, Y., et al., 2019. Soil health assessment: a critical review of current methodologies and a proposed new approach. Sci. Total Environ. 648, 1484–1491.
Running, S., Nemani, R., Heinsch, F., et al., 2004. A continuous satellite-derived measure of global terrestrial primary production. Bioscience 54 (6), 547–560.
Sato, H., 2001. The current state of Paddy agriculture in Japan. Irrigat. Drain.: J. Int. Commiss. Irrigat. Drain. 50 (2), 91–99.
Swanepoel, P., Du Preez, C., Botha, P., et al., 2014. Soil quality characteristics of kikuyu–ryegrass pastures in South Africa. Geoderma 232, 589–599.
Tao, F., Zhang, Z., 2013. Climate change, high-temperature stress, rice productivity, and water use in eastern China: a new superensemble-based probabilistic projection. J. Appl. Meteorol. Climatol. 52 (3), 531–551.
Tao, S., Wei, J., Sun, J., et al., 2009. The severe drought in East China during November, December and January 2008–2009. Meteorol. Monthly 35 (04), 3–10 (in Chinese with English abstract).
Viana, C., Freire, D., Abrantes, P., et al., 2022. Agricultural land systems importance for supporting food security and sustainable development goals: a systematic review. Sci. Total Environ. 806, 150718.
Wan, C., Kuzyakov, Y., Cheng, C., et al., 2021. A soil sampling design for arable land quality observation by using SPCOSA–CLHS hybrid approach. Land Degrad. Dev. 32 (17), 4889–4906.
Wang, J., 2017. Geodetector: principle and prospective. Acta Geograph. Sin. 72 (1) (in Chinese with English abstract).
Wang, J., Hu, Y., 2012. Environmental health risk detection with GeogDetector. Environ. Model Softw. 33 (7), 114–115.
Wang, K., Zhang, P., 2013. The research on impact factors and characteristic of cultivated land resources use efficiency—take Henan province, China as a case study. Ieri Procedia 5, 2–9.
Wang, Z., Zhao, Y., Liao, Q., et al., 2008. Spatio-temporal variation and associated affecting factors of soil pH in the past 20 years of Jiangsu Province, China. Acta Ecol. Sin. 02, 720–727 (in Chinese with English abstract).
Wang, J., Li, X., Christakos, G., et al., 2010. Geographical detectors-based health risk assessment and its application in the neural tube defects study of the Heshun region, China. Int. J. Geogr. Inf. Sci. 24 (1), 107–127.
Wang, J., Zhang, T., Fu, B., 2016. A measure of spatial stratified heterogeneity. Ecol. Indic. 67, 250–256.
Wang, X., Xia, J., Li, Q., et al., 2023. Spatiotemporal variation of flood distribution and influencing factors in provinces in middle and lower reaches of Yangtze River. Water Resourc. Protect. 39 (02), 78–86 (in Chinese with English abstract).
Wang, J., Haining, R., Zhang, T., et al., 2024. Statistical modeling of spatially stratified heterogeneous data. Ann. Am. Assoc. Geogr. 114 (3), 499–519.
Wei, L., Zhu, Z., Razavi, B., et al., 2022. Visualization and quantification of carbon "rusty sink" by rice root iron plaque: mechanisms, functions, and global implications. Glob. Chang. Biol. 28 (22), 6711–6727. https://doi.org/10.1111/gcb.16372.
Xiao, L., Wang, G., Wang, E., et al., 2024. Spatiotemporal co-optimization of agricultural management practices towards climate-smart crop production. Nat. Food 5, 59–71.
Xu, M., 2020. Current application status, existing problems, and development strategies of high-quality rice varieties in Jiangsu Province. China Rice 26 (04), 57–60 (in Chinese with English abstract).

Xu, Y., Pu, L., Zhang, R., et al., 2017. Cropland quality evolution following coastal reclamation at the prograding tidal flats of Jiangsu Province, China. Acta Geograph. Sin. 72 (11), 2032–2046 (in Chinese with English abstract).
Yang, C., Everitt, J., 2012. Using spectral distance, spectral angle and plant abundance derived from hyperspectral imagery to characterize crop yield variation. Precis. Agric. 13, 62–75.
Ye, S., Zhu, D., Yao, X., et al., 2014. Development of a highly flexible mobile GIS-based system for collecting arable land quality data. IEEE Jo. Sel. Top. Appl. Earth Observa. Rem. Sens. 7, 4432–4441.
Ye, S., Song, C., Cheng, F., et al., 2019. Cultivated land health-productivity comprehensive evaluation and its pilot evaluation in China. Trans. Chin. Soc. Agric. Eng. 35 (22), 66–78 (in Chinese with English abstract).
Ye, S., Song, C., Shen, S., et al., 2020. Spatial pattern of arable land-use intensity in China. Land Use Policy 99, 104845.
Ye, S., Song, C., Ren, S., et al., 2022a. Spatial patterns of county-level arable land productive-capacity and its coordination with land-use intensity in mainland China. Agric. Ecosyst. Environ. 326, 107757.
Ye, S., Song, C., Gao, P., et al., 2022b. Visualizing clustering characteristics of multidimensional arable land quality indexes at the county level in mainland China. Environ. Plann. A: Econ. Space 54 (2), 222–225.
Ye, S., Song, C., Gao, P., et al., 2023. Construction of the new cognitive system for arable land resources from geospatial perspective. Trans. Chin. Soc. Agric. Eng. 39 (9), 225–240 (in Chinese with English abstract).
Ye, S., Wang, J., Jiang, J., et al., 2024a. Coupling input and output intensity to explore the sustainable agriculture intensification path in mainland China. J. Clean. Prod. 442, 140827.
Ye, S., Ren, S., Song, C., et al., 2024b. Spatial pattern of cultivated land fragmentation in mainland China: characteristics, dominant factors, and countermeasures. Land Use Policy 139, 107070.
Yu, Q., Hu, Q., Wu, H., et al., 2024a. View from above: farmland infrastructure and its impacts on agricultural landscapes. Innovat. Geosci. 3, 100107.
Yu, W., Li, D., Zheng, H., et al., 2024b. HIDYM: a high-resolution gross primary productivity and dynamic harvest index based crop yield mapper. Remote Sens. Environ. 311, 114301.
Zhang, G., 1988. Relationship between clay content and soil fertility in paddy soils. Jiangsu Agric. Sci. 12, 17–19 (in Chinese).
Zhang, H., Zhou, S., Wu, S., et al., 2010. Provincial scale spatial variation of cultivated land production capacity and its impact factors. Trans. Chin. Soc. Agric. Eng. 26 (8), 308–314 (in Chinese with English abstract).
Zhang, B., Guo, F., Huang, D., et al., 2020. Pattern and evaluation of land consolidation model for “one household one plot” and “one village one plot” to solve land fragmentation in northern Shaanxi Province, China. Trans. Chin. Soc. Agric. Eng. (Trans. CSAE) 36 (15), 28–36 (in Chinese with English abstract).
Zhang, R., Ye, S., Ren, S., 2024. Spatial pattern and driving factors of cultivated land fragmentation in Jiangsu Province using MGWR model. Trans. Chin. Soc. Agric. Eng. 40 (16), 229–239 (in Chinese with English abstract).
Zhao, S., Ji, S., Wang, S., et al., 2004. Relationship between different soil types and the quality and yield of strong-gluten wheat. Henan Agric. Sci. 7, 52–53 (in Chinese).
Zhao, M., Zhang, G., Li, D., et al., 2013. Spatial variation of soi organic matter and its main influencing factors in Jangsu Province. Acta Ecol. Sin. 33 (16), 5058–5066 (in Chinese with English abstract).
Zhou, S., Chen, G., Fang, L., et al., 2016. GIS-based integration of subjective and objective weighting methods for regional landslides susceptibility mapping. Sustainability 8 (4), 334.
Zhou, Y., Li, X., Liu, Y., 2020. Land use change and driving factors in rural China during the period 1995–2015. Land Use Policy 99, 105048.